Frontiers of Physics
https://doi.org/10.1007/s11467-019-0934-z
Front. Phys.
15(2), 22601 (2020)

RESEARCH ARTICLE

Reflection and refraction of elastic wave at VTI-TTI media interface

Lin Fa[1,†], Jiaojiao Tang[1], Qi Zhang[1], Minjin Zhang[1], Yandong Zhang[1], Meng Liang[1], Meishan Zhao[2]

[1] *School of Electronic Engineering, Xi'an University of Posts and Telecommunications, Xi'an 710121, China*
[2] *James Franck Institute and Department of Chemistry, The University of Chicago, Chicago, IL 60637, USA*
Corresponding author. Email: †faxiaoxue@1216.com
Received August 6, 2019; accepted October 8, 2019

We explore the physical phenomenon of acoustic waves induced at the interface between two different anisotropic rock media. Specifically, one medium is a transversely isotropic medium with a vertical axis of symmetry (VTI medium) and the other one is a transversely isotropic medium with a tilt axis of symmetry (TTI medium). By solving the Kelvin–Christoffel equation, an eighth-order polynomial is established for reflection and refraction angles, which is confirmed from Snell's law. Three types of analytical expressions of the polarization coefficients of the induced waves are obtained corresponding to different incident angle regions. An effective algorithm has been developed for numerical analysis of the polarization coefficients. Applying characteristic anisotropic parameters reported in the literature, the influencing factors on reflection and refraction coefficients are analyzed, e.g., the anisotropy, the tilt-angle of rock-layer, and the incident-angle. The calculated reflection and refraction coefficients have been rechecked for energy conservation.

Keywords VTI-TTI interface, reflection, refraction, rock anisotropy, tilt-angle

1 Introduction

A comprehensive understanding of reflection and refraction of acoustic waves at an interface between two different media is fundamentally important in acoustics. Scientific and industrial applications have been extensive in this regard, e.g., AVO (amplitude variations with offset) analysis of seismic data in petroleum industry [1], wave energy device development [2], rangefinder [3], medical imaging [4], nondestructive detection [5–7], underwater acoustics detection [8], unidirectional transmission of acoustic waves [9], the design of substrate in some acoustic devices [10], SAW technology [11], and more. Although acoustic wave has its own distinctive characteristics that are different from those of optic wave, they have many similarities. For example, similar to optic waves [12], acoustic waves can create negative refraction [13]. The transformational optical technology is based on the reflection and refraction of optic wave. This optics method can also be introduced to manipulate acoustic waves [14]. Reflection and refraction of the waves are important issues for both acoustics and optics.

Zoeppritz [15] reported analytic solutions of reflection and refraction coefficients for interface between two isotropic media and provided a set of equations to describe the amplitudes of the reflected and refracted waves. Due to its algebraic complexity, the solution for reflection coefficients was mostly given as an approximation in geophysical exploration. For instance, in solving inverse problems for the properties and structure of underground strata from the reflection signature, it was mostly using an approximate analytic expression. Meanwhile, several approximate expressions of reflection and refraction coefficients were reported under different physical assumptions for isotropic models, e.g., by Richards and Fraisier [16], Aki and Richards [17], and Shuey [18].

The amplitude of P-wave could be affected by acoustic impedances of the media on both sides of the interface. Ostrander [19] showed that AVO anomalies could identify the areas of Poisson's ratio change. So, they could be used as hydrocarbon indicators. Conventional AVO inverse of reflected seismic waves was conducted by Li *et al.* [20]. To our understanding, most of the published literature on applications of reflection and refraction involved only the amplitude information of the reflection coefficients. Within the limited reports on discussions of phase information of reflection coefficient in acoustic-logging and seismic-exploration, Zhu *et al.* [21] reported an experimental study on lateral-displacement of the reflection P-wave, and Fa *et al.* [22] showed that phase information of reflection coefficient could be used to calibrate experimental data, i.e., both the seismic exploration data for accurate time-depth conversion in post-incident critical-angle region and the acoustic logging data for accurate measurement of propagation speed of P-wave along borehole wall. Nevertheless, all the reported discussions were limited to the systems within an isotropic rock-layer.

The interior of the earth is usually composed of a series of isotropic, regular thin layers with different properties. A seismic wavelength is usually much longer than the thickness of each layer in the strata. A sequence of strata

© Higher Education Press and Springer-Verlag GmbH Germany, part of Springer Nature 2020

with a vertical-axis symmetry was named a VTI medium whose macroscopic anisotropy and mechanical property could be described by an elastic tensor of hexagonal crystal system [23–25]. Anisotropic behavior of layered underground strata at the macroscopic level was predicted by Backus [26]. This macroscopic anisotropy was assumed to be transversely isotropic which could influence significantly on seismic waves with respect to propagation, reflection, refraction, and polarization. Applications to the field of geosciences have been widely reported. Thomson [23] and Wang [24, 25] reported some measured rock anisotropy parameters and provided a connection between rock anisotropy parameters and stiffness matrix elements of a hexagonal system. Studies of reflection coefficients between two VTI media have been reported from several research groups, e.g., Daley *et al.* [27, 28], Rüger [29], Tsvankin [30], Carcione [31], and Klimeš [32]. A fourth-order polynomial in the analysis of the reflection and refraction angles was established for the VTI-VTI interface by Fa *et al.* [33, 34] and an efficient algorithm for numerical calculations was also developed.

Realistically, the symmetric axis of a sequence of thin-layers may not be parallel to the vertical axis. Instead, the sequence consists of tilt rock-layers. This macroscopic structure with anisotropy is named as a TTI medium model. Based on our knowledge of VTI medium [36–45], a stiffness matrix form of VTI medium may be obtained from the stiffness matrix of TTI medium through Bond transformation in rotational coordinates [35]. Through inverse transformations, the stiffness matrix of a VTI medium can also be transformed back into the stiffness matrix form of a TTI medium.

In this paper, we report the studies about the effects of the various system parameters on reflection and refraction coefficients at VTI-TTI media interface, e.g., incident-angle, physical and anisotropic parameters, and tilt-angle of TTI medium.

2 Modeling

Considering an interface between VTI and TTI media, Fig. 1 shows a schematic structural sketch of the two anisotropy rocks.

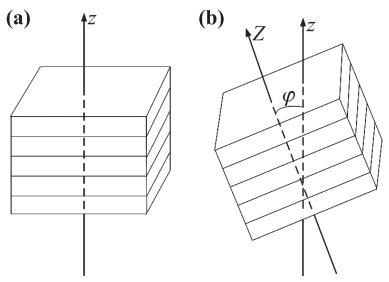


Fig. 1 A schematic sketch of VTI and TTI anisotropic rock models: **(a)** VTI medium model; **(b)** TTI medium model.

The anisotropic and mechanical properties of a VTI medium can be expressed in a stiff matrix [23–25]:

$$C^{(V)}=\begin{pmatrix} c_{11}^{(V)} & c_{12}^{(V)} & c_{13}^{(V)} & 0 & 0 & 0 \\ c_{12}^{(V)} & c_{11}^{(V)} & c_{13}^{(V)} & 0 & 0 & 0 \\ c_{13}^{(V)} & c_{13}^{(V)} & c_{33}^{(V)} & 0 & 0 & 0 \\ 0 & 0 & 0 & c_{44}^{(V)} & 0 & 0 \\ 0 & 0 & 0 & 0 & c_{44}^{(V)} & 0 \\ 0 & 0 & 0 & 0 & 0 & c_{66}^{(V)} \end{pmatrix}, \quad (1)$$

where there are five independent elements and $c_{12}^{(V)}=c_{11}^{(V)}-2c_{66}^{(V)}$. By Bond transformation [35] with a rotating angle φ, it yields a stiff matrix form for TTI media:

$$\begin{aligned} C^{(T)} &= GC^{(V)}J^{-1} \\ &= \begin{pmatrix} c_{11}^{(T)} & c_{12}^{(T)} & c_{13}^{(T)} & 0 & c_{15}^{(T)} & 0 \\ c_{12}^{(T)} & c_{11}^{(T)} & c_{23}^{(T)} & 0 & c_{25}^{(T)} & 0 \\ c_{13}^{(T)} & c_{23}^{(T)} & c_{33}^{(T)} & 0 & c_{35}^{(T)} & 0 \\ 0 & 0 & 0 & c_{44}^{(T)} & 0 & c_{46}^{(T)} \\ c_{15}^{(T)} & c_{25}^{(T)} & c_{35}^{(T)} & 0 & c_{55}^{(T)} & 0 \\ 0 & 0 & 0 & c_{46}^{(T)} & 0 & c_{66}^{(T)} \end{pmatrix}. \end{aligned} \quad (2)$$

The two transformation matrices and related elements are

$$G=\begin{pmatrix} \cos^2\varphi & 0 & \sin^2\varphi & 0 & -\sin 2\varphi & 0 \\ 0 & 1 & 0 & 0 & 0 & 0 \\ \sin^2\varphi & 0 & \cos^2\varphi & 0 & \sin 2\varphi & 0 \\ 0 & 0 & 0 & \cos\varphi & 0 & \sin\varphi \\ (\sin 2\varphi)/2 & 0 & -(\sin 2\varphi)/2 & 0 & \cos 2\varphi & 0 \\ 0 & 0 & 0 & -\sin\varphi & 0 & \cos\varphi \end{pmatrix}, \quad (3)$$

$$J^{-1}=\begin{pmatrix} \cos^2\varphi & 0 & \sin^2\varphi & 0 & -(\sin 2\varphi)/2 & 0 \\ 0 & 1 & 0 & 0 & 0 & 0 \\ \sin^2\varphi & 0 & \cos^2\varphi & 0 & (\sin 2\varphi)/2 & 0 \\ 0 & 0 & 0 & \cos\varphi & 0 & \sin\varphi \\ \sin 2\varphi & 0 & -\sin 2\varphi & 0 & \cos 2\varphi & 0 \\ 0 & 0 & 0 & -\sin\varphi & 0 & \cos\varphi \end{pmatrix}, \quad (4)$$

where

$$\begin{aligned} c_{11}^{(T)} &= c_{11}^{(V)}\cos^4\varphi + c_{33}^{(V)}\sin^4\varphi + [(c_{13}^{(V)}+2c_{44}^{(V)})\sin^2 2\varphi]/2, \\ c_{12}^{(T)} &= c_{12}^{(V)}\cos^2\varphi + c_{13}^{(V)}\sin^2\varphi, \\ c_{13}^{(T)} &= c_{13}^{(V)}(\sin^4\varphi+\cos^4\varphi) + [(c_{11}^{(V)}+c_{33}^{(V)})/4 - c_{44}^{(V)}]\sin^2 2\varphi, \end{aligned}$$

$$
\begin{aligned}
c_{15}^{(T)} &= \{[(c_{11}^{(V)} - c_{13}^{(V)})\cos^2\varphi + (c_{13}^{(V)} - c_{33}^{(V)})\sin^2\varphi]/2 \\
&\quad - c_{44}^{(V)}\cos 2\varphi\}\sin 2\varphi, \\
c_{23}^{(T)} &= c_{12}^{(V)}\sin^2\varphi + c_{13}^{(V)}\cos^2\varphi, \\
c_{25}^{(T)} &= [(c_{12}^{(V)} - c_{13}^{(V)})\sin 2\varphi]/2, \\
c_{33}^{(T)} &= c_{11}^{(V)}\sin^4\varphi + c_{33}^{(V)}\cos^4\varphi + (c_{13}^{(V)}/2 + c_{44}^{(V)})\sin^2 2\varphi, \\
c_{35}^{(T)} &= \{[(c_{11}^{(V)} - c_{13}^{(V)})\sin^2\varphi + (c_{13}^{(V)} - c_{33}^{(V)})\cos^2\varphi]/2 \\
&\quad + c_{44}^{(V)}\cos 2\varphi\}\sin 2\varphi, \\
c_{44}^{(T)} &= c_{44}^{(V)}\cos^2\varphi + c_{66}^{(V)}\sin^2\varphi, \\
c_{46}^{(T)} &= [(c_{66}^{(V)} - c_{44}^{(V)})\sin 2\varphi]/2, \\
c_{55}^{(T)} &= [(c_{11}^{(V)} + c_{33}^{(V)} - 2c_{13}^{(V)})\sin^2 2\varphi]/4 + c_{44}^{(V)}\cos^2 2\varphi, \\
c_{66}^{(T)} &= c_{44}^{(V)}\sin^2\varphi + c_{66}^{(V)}\cos^2\varphi.
\end{aligned}
$$

Now, let's consider the VTI-TTI interface at the x–y plane, as shown in Fig. 2. The upside of the interface (x–y plane) is a VTI medium and the underside is TTI medium. The angle between the symmetric-axis of TTI and the z-axis is φ, shown in Fig. 2(a). When an incident P-wave is propagating onto the interface, several additional waves are induced, i.e., a reflected P-wave, a refracted P-wave, a reflected SV-wave, and a refracted SV-wave. The particle displacements of the incident and the induced waves are parallel to the x–z plane, shown in Fig. 2(b). The polarization directions of P-wave and SV-wave at a given spatial location are perpendicular to each other [35]; if they are not at the same space location, they do not have to be perpendicular. Generally, these waves are neither purely longitudinal nor purely transverse.

For a harmonic vibrational motion of a particle with angular frequency ω, the particle displacement of the incident P-wave can be written as

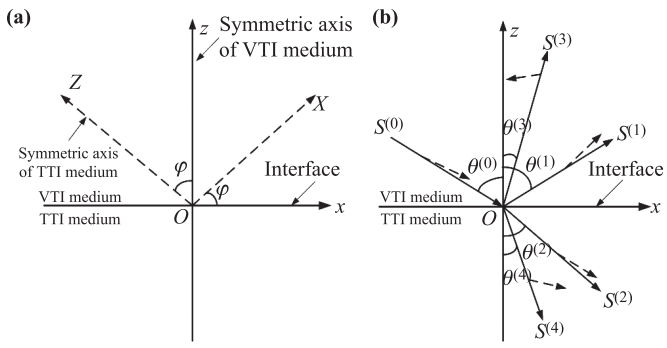


Fig. 2 Schematic representation of VTI-TTI media interface: **(a)** showing the angle between the symmetric-axis of VTI medium and that of TTI medium, where the z-axis is the symmetric-axis of VTI medium and normal to the interface, and Z-axis is that of TTI medium; **(b)** geometry of wavefront normal and polarization directions for the incident and converted waves at the interface. The arrowheads on the long-lines indicate the directions of phase velocity and those on the short-lines indicate the polarization direction.

$$
\begin{aligned}
S^{(0)} &= R^{(0)}\begin{pmatrix} u_{xo}^{(0)} \\ -u_{zo}^{(0)} \end{pmatrix}\exp[\mathrm{i}(\omega t - k^{(0)}x\sin\theta + k^{(0)}z\cos\theta)] \\
&= |R^{(0)}|\begin{pmatrix} u_{x}^{(0)} \\ -u_{z}^{(0)} \end{pmatrix}\exp[\mathrm{i}(\omega t - k^{(0)}x\sin\theta + k^{(0)}z\cos\theta)].
\end{aligned} \tag{5}
$$

The particle displacements of the four induced waves can be written as

$$
\begin{aligned}
S^{(1)} &= R^{(1)}\begin{pmatrix} u_{xo}^{(1)} \\ u_{zo}^{(1)} \end{pmatrix}\exp[\mathrm{i}(\omega t - k^{(1)}x\sin\theta^{(1)} - k^{(1)}z\cos\theta^{(1)})] \\
&= |R^{(1)}|\begin{pmatrix} u_{x}^{(1)} \\ u_{z}^{(1)} \end{pmatrix}\exp[\mathrm{i}(\omega t - k^{(1)}x\sin\theta^{(1)} - k^{(1)}z\cos\theta^{(1)})],
\end{aligned} \tag{6}
$$

$$
\begin{aligned}
S^{(2)} &= R^{(2)}\begin{pmatrix} u_{xo}^{(2)} \\ -u_{zo}^{(2)} \end{pmatrix}\exp[\mathrm{i}(\omega t - k^{(2)}x\sin\theta^{(2)} + k^{(2)}z\cos\theta^{(2)})] \\
&= |R^{(2)}|\begin{pmatrix} u_{x}^{(2)} \\ -u_{z}^{(2)} \end{pmatrix}\exp[\mathrm{i}(\omega t - k^{(2)}x\sin\theta^{(2)} + k^{(2)}z\cos\theta^{(2)})],
\end{aligned} \tag{7}
$$

$$
\begin{aligned}
S^{(3)} &= R^{(3)}\begin{pmatrix} -u_{zo}^{(3)} \\ -u_{xo}^{(3)} \end{pmatrix}\exp[\mathrm{i}(\omega t - k^{(3)}x\sin\theta^{(3)} - k^{(3)}z\cos\theta^{(3)})] \\
&= |R^{(3)}|\begin{pmatrix} -u_{z}^{(3)} \\ -u_{x}^{(3)} \end{pmatrix}\exp[\mathrm{i}(\omega t - k^{(3)}x\sin\theta^{(3)} - k^{(3)}z\cos\theta^{(3)})],
\end{aligned} \tag{8}
$$

$$
\begin{aligned}
S^{(4)} &= R^{(4)}\begin{pmatrix} -u_{zo}^{(4)} \\ u_{xo}^{(4)} \end{pmatrix}\exp[\mathrm{i}(\omega t - k^{(4)}x\sin\theta^{(4)} + k^{(4)}z\cos\theta^{(4)}) \\
&= |R^{(4)}|\begin{pmatrix} -u_{z}^{(4)} \\ u_{x}^{(4)} \end{pmatrix}\exp[\mathrm{i}(\omega t - k^{(4)}x\sin\theta^{(4)} + k^{(4)}z\cos\theta^{(4)})],
\end{aligned} \tag{9}
$$

and

$$
\begin{aligned}
\begin{pmatrix} u_{x}^{(m)} \\ u_{z}^{(m)} \end{pmatrix} &= \begin{pmatrix} u_{xo}^{(m)} \\ u_{zo}^{(m)} \end{pmatrix}\exp[\mathrm{i}\phi^{(m)}] \\
&= \begin{pmatrix} |u_{xo}^{(m)}|\exp[\mathrm{i}\gamma_{x}^{(m)}] \\ |u_{zo}^{(m)}|\exp[\mathrm{i}\gamma_{z}^{(m)}] \end{pmatrix}\exp[\mathrm{i}\phi^{(m)}] \\
&= \begin{pmatrix} |u_{xo}^{(m)}|(\cos\phi_{x}^{(m)} + \mathrm{i}\sin\phi_{x}^{(m)}) \\ |u_{zo}^{(m)}|(\cos\phi_{z}^{(m)} + \mathrm{i}\sin\phi_{z}^{(m)}) \end{pmatrix} \\
&= \begin{pmatrix} a_{1}^{(m)} + \mathrm{i}b_{1}^{(m)} \\ a_{3}^{(m)} + \mathrm{i}b_{3}^{(m)} \end{pmatrix},
\end{aligned} \tag{10}
$$

where the superscripts $\{m\} = \{0, 1, 2, 3, 4\}$ denote the cases of the incident P-wave ($m = 0$), reflected P-waves ($m = 1$), refracted ($m = 2$) P-waves, reflected SV-waves ($m = 3$), and refracted SV-waves ($m = 4$); $\theta^{(m)}$ is an incidence/reflection/refraction angle for the corresponding wave; $R^{(m)} = |R^{(m)}|\exp[\mathrm{i}\phi^{(m)}]$; $\phi_{x}^{(m)} = \phi^{(m)} + \gamma_{x}^{(m)}$ and $\phi_{z}^{(m)} = \phi^{(m)} + \gamma_{z}^{(m)}$, for induced homogenous wave

$\phi_x^{(m)} = \phi_z^{(m)} = \phi^{(m)}$ due to $\gamma_x^{(m)} = \gamma_z^{(m)} = 0$; for induced inhomogenous wave $\phi_x^{(m)} \neq \phi_z^{(m)}$ and both of them have the phase difference of $\pi/2$; $u_{xo}^{(m)}$ and $u_{zo}^{(m)}$ are polarization coefficients of each wave without considering the phase shift caused by reflection/refraction; $R^{(1)}$ is the reflection coefficient of P-wave to P-wave; $R^{(2)}$ is the refraction coefficient of P-wave to P-wave; $R^{(3)}$ is the reflection coefficient of P-wave to SV-wave, $R^{(4)}$ is the refraction coefficient of P-wave to SV-wave; and $R^{(0)} = 1$.

Let us consider a few cases, which are classified based on incidence angle: the first case is the incidence in a system without any critical-angle; the second one is the incidence from the pre-critical-angle region in a system where there is a critical incidence-angle corresponding to refracted P-wave, and the third case is the incidence from the post-critical-angle region. In the first two cases, the phase factor $\phi^{(1,3)}$ is either 0° or 180°. The selection of a phase angle is determined by the acoustic impedance of the media involved in the interface. The third case is the one in the post-critical-angle region which will be discussed next in detail.

2.1 Phase velocity solutions of incident and induced waves at VTI-TTI interface

In the following, we derive an analytic expression of polarization coefficients and phase velocity and propose an efficient algorithm in calculations of reflection and refraction coefficients at VTI-TTI interface.

In absence of external forces, the Kelvin–Christoffel equation can be simplified for incident wave and four induced waves at VTI-TTI interface

$$\begin{bmatrix} \Gamma_{11}^{(m)} - [v^{(m)}]^2 & \Gamma_{13}^{(m)} \\ \Gamma_{31}^{(m)} & \Gamma_{33}^{(m)} - [v^{(m)}]^2 \end{bmatrix} \begin{bmatrix} u_x^{(m)} \\ u_z^{(m)} \end{bmatrix} = 0. \tag{11}$$

Within VTI incidence medium which is denoted by a superscript V, the matrix elements are given by [33, 34]

$$\Gamma_{11}^{(0,1,3)} = A_{11}^{(V)} \sin^2\theta^{(0,1,3)} + A_{44}^{(V)} \cos^2\theta^{(0,1,3)}, \tag{12}$$

$$\Gamma_{13}^{(0,1,3)} = \Gamma_{31}^{(0,1,3)} = [A_{13}^{(V)} + A_{44}^{(V)}] \sin\theta^{(0,1,3)} \cos\theta^{(0,1,3)}, \tag{13}$$

$$\Gamma_{33}^{(0,1,3)} = A_{33}^{(V)} \cos^2\theta^{(0,1,3)} + A_{44}^{(V)} \sin^2\theta^{(0,1,3)}. \tag{14}$$

The phase velocity solutions of incident P-wave and reflected P- and SV-waves are

$$v_{1,2}^{(0,1,3)} = \{[A_4^{(V)} \sin^2\theta^{(0,1,3)} + A_5^{(V)} \pm Q^{(V)}(\theta^{(0,1,3)})]/2\}^{1/2}, \tag{15}$$

$$Q^{(V)}(\theta^{(0,1,3)}) = [(A_1^{(V)} \sin^2\theta^{(0,1,3)} + A_2^{(V)} \cos^2\theta^{(0,1,3)})^2 + (A_3^{(V)})^2 \sin^2 2\theta^{(0,1,3)}]^{1/2}, \tag{16}$$

where $\rho^{(V)}$ is the density of VTI medium; the subscripts $\{1,2,3,4,5,6\} = \{j,l\}$, where the subscripts 1 and 2 indicate two different solutions of the phase velocity; and $A_1^{(V)} = A_{11}^{(V)} - A_{44}^{(V)}$, $A_2^{(V)} = A_{44}^{(V)} - A_{33}^{(V)}$, $A_3^{(V)} = A_{13}^{(V)} + A_{44}^{(V)}$, $A_4^{(V)} = A_{11}^{(V)} - A_{33}^{(V)}$, $A_5^{(V)} = A_{33}^{(V)} + A_{44}^{(V)}$, and $A_{jl}^{(V)} = C_{jl}^{(V)}/\rho^{(V)}$.

Within the refraction medium TTI, the matrix elements are given by

$$\Gamma_{11}^{(2,4)} = A_{11}^{(T)} \sin^2\theta^{(2,4)} + A_{15}^{(T)} \sin 2\theta^{(2,4)} + A_{55}^{(T)} \cos^2\theta^{(2,4)}, \tag{17}$$

$$\Gamma_{13}^{(2,4)} = \Gamma_{31}^{(2,4)} = (A_{13}^{(T)} + A_{55}^{(T)}) \sin 2\theta^{(2,4)}/2 + A_{35}^{(T)} \cos^2\theta^{(2,4)} + A_{15}^{(T)} \sin^2\theta^{(2,4)}, \tag{18}$$

$$\Gamma_{33}^{(2,4)} = A_{33}^{(T)} \cos^2\theta^{(2,4)} + A_{35}^{(T)} \sin 2\theta^{(2,4)} + A_{55}^{(T)} \sin^2\theta^{(2,4)}, \tag{19}$$

and the phase velocity solutions of the refracted P- and SV-waves

$$v_{1,2}^{(2,4)} = \{[c_1 \sin^2\theta^{(2,4)} + c_2 \sin 2\theta^{(2,4)} + c_3 \cos^2\theta^{(2,4)} \pm Q^{(T)}(\theta^{(2,4)})]/2]\}^{1/2}, \tag{20}$$

$$Q^{(T)}(\theta^{(2,4)}) = [b_1 \sin^4\theta^{(2,4)} + b_2 \cos^4\theta^{(2,4)} + b_3 \sin^2 2\theta^{(2,4)} + \sin 2\theta^{(2,4)}(b_4 \sin^2\theta^{(2,4)} + b_5 \cos^2\theta^{(2,4)})]^{1/2}, \tag{21}$$

where $\rho^{(T)}$ is the density of TTI medium; the subscripts 1 and 2 of $v_{1,2}^{(2,4)}$ indicate that there are two solutions; and $a_1 = A_{11}^{(T)} - A_{55}^{(T)}$, $a_2 = A_{15}^{(T)} - A_{35}^{(T)}$, $a_3 = A_{55}^{(T)} - A_{33}^{(T)}$, $a_4 = (A_{13}^{(T)} + A_{55}^{(T)})/2$, $b_1 = a_1^2 + 4[A_{15}^{(T)}]^2$, $b_2 = a_3^2 + 4[A_{35}^{(T)}]^2$, $b_3 = a_1 a_3/2 + a_2^2 + 4a_4^2 + 2A_{15}^{(T)} A_{35}^{(T)}$, $b_4 = 2(a_1 a_2 + 4a_4 A_{15}^{(T)})$, $b_5 = 2(a_2 a_3 + 4a_4 A_{35}^{(T)})$, $c_1 = A_{11}^{(T)} + A_{55}^{(T)}$, $c_2 = A_{15}^{(T)} + A_{35}^{(T)}$, $c_3 = A_{33}^{(T)} + A_{55}^{(T)}$, and $A_{ji}^{(T)} = c_{ji}^{(T)}/\rho^{(T)}$.

The selection of a phase velocity from these two possible solutions [Eqs. (15) and (20)] depends on the nature of the induced wave.

2.2 Determination of z-components of power density flux

To derive an analytical expression for polarization coefficients of the inhomogeneous wave which is induced at the interface, let us first calculate the real parts of the fluxes for the z-components of incident P-wave and the induced waves.

The relationship amongst stress, particle displacement, and corresponding particle vibration velocity is given by [35]

$$T^{(m)} = C^{(n)} : \nabla_s S^{(m)} \tag{22}$$

with a harmonic vibration

$$V^{(m)} = \frac{\partial S^{(m)}}{\partial t} = \mathrm{i}\omega S^{(m)}, \tag{23}$$

where the sign ":" is a tensor product operator; the sign "∇_s" is a gradient operator; and the superscripts $\{n\} = \{V,T\}$ stand for VTI medium and TTI medium, respectively.

For incident P-wave, reflected P- and SV-waves propagating on the x–z plane within VTI medium, Eq. (22) can be written explicitly as

$$\begin{pmatrix} T_1^{(m)} \\ T_2^{(m)} \\ T_3^{(m)} \\ T_4^{(m)} \\ T_5^{(m)} \\ T_6^{(m)} \end{pmatrix} = \begin{pmatrix} c_{11}^{(V)} & c_{12}^{(V)} & c_{13}^{(V)} & 0 & 0 & 0 \\ c_{12}^{(V)} & c_{11}^{(V)} & c_{13}^{(V)} & 0 & 0 & 0 \\ c_{13}^{(V)} & c_{13}^{(V)} & c_{33}^{(V)} & 0 & 0 & 0 \\ 0 & 0 & 0 & c_{44}^{(V)} & 0 & 0 \\ 0 & 0 & 0 & 0 & c_{44}^{(V)} & 0 \\ 0 & 0 & 0 & 0 & 0 & c_{66}^{(V)} \end{pmatrix} \begin{pmatrix} \partial/\partial x & 0 & 0 \\ 0 & 0 & 0 \\ 0 & 0 & \partial/\partial z \\ 0 & \partial/\partial z & 0 \\ \partial/\partial z & & \partial/\partial x \\ 0 & \partial/\partial x & 0 \end{pmatrix} \begin{pmatrix} S_x^{(m)} \\ 0 \\ S_z^{(m)} \end{pmatrix} = \begin{pmatrix} c_{11}^{(V)}\partial S_x^{(m)}/\partial x + c_{13}^{(V)}\partial S_z^{(m)}/\partial z \\ c_{12}^{(V)}\partial S_x^{(m)}/\partial x + c_{13}^{(V)}\partial S_z^{(m)}/\partial z \\ c_{13}^{(V)}\partial S_x^{(m)}/\partial x + c_{33}^{(V)}\partial S_z^{(m)}/\partial z \\ 0 \\ c_{44}^{(V)}(\partial S_x^{(m)}/\partial z + \partial S_z^{(m)}/\partial x) \\ 0 \end{pmatrix}, \tag{24}$$

where $\{m\} = \{0, 1, 3\}$ are for incident P-wave, reflected P- and SV-waves; $S_x^{(m)}$ and $S_z^{(m)}$ are x- and z-components.

The power density flux of the incident P-wave and the reflected P- and SV-waves can be written as

$$P^{(m)} = -\frac{[V^{(m)}]^* \cdot T^{(m)}}{2} = -\frac{1}{2}\begin{pmatrix} [V_x^{(m)}]^* T_1^{(m)} + [V_z^{(m)}]^* T_5^{(m)} \\ 0 \\ [V_x^{(m)}]^* T_5^{(m)} + [V_z^{(m)}]^* T_3^{(m)} \end{pmatrix}, \tag{25}$$

where the sign "$\cdot$" is the dot product operator. The stress related to z-components of density fluxes of the incident P-wave, and reflected P- and SV-waves are written as

$$T_3^{(0)} = -\mathrm{i}k^{(0)}(c_{13}^{(V)}u_{xo}^{(0)}\sin\theta + c_{33}^{(V)}u_{zo}^{(0)}\cos\theta)\exp[\mathrm{i}(\omega t - k^{(0)}x\sin\theta - k^{(0)}z\cos\theta)], \tag{26}$$
$$T_5^{(0)} = \mathrm{i}k^{(0)}c_{44}(u_{xo}^{(0)}\cos\theta + u_{zo}^{(0)}\sin\theta)\exp[\mathrm{i}(\omega t - k^{(0)}x\sin\theta - k^{(0)}z\cos\theta)], \tag{27}$$
$$T_3^{(1)} = -\mathrm{i}k^{(1)}|R^{(1)}|(c_{13}^{(V)}u_{xo}^{(1)}\sin\theta + c_{33}^{(V)}u_{zo}^{(1)}\cos\theta)\exp[\mathrm{i}(\omega t - k^{(1)}x\sin\theta^{(1)} - k^{(1)}z\cos\theta^{(1)} + \phi^{(1)})], \tag{28}$$
$$T_5^{(1)} = -\mathrm{i}k^{(1)}c_{44}|R^{(1)}|(u_{xo}^{(1)}\cos\theta + u_{zo}^{(1)}\sin\theta)\exp[\mathrm{i}(\omega t - k^{(1)}x\sin\theta^{(1)} - k^{(1)}z\cos\theta^{(1)} + \phi^{(1)})], \tag{29}$$
$$T_3^{(3)} = \mathrm{i}k^{(3)}|R^{(3)}|(c_{13}^{(V)}u_{xo}^{(3)}\sin\theta + c_{33}^{(V)}u_{zo}^{(3)}\cos\theta)\exp[\mathrm{i}(\omega t - k^{(3)}x\sin\theta^{(3)} - k^{(3)}z\cos\theta^{(3)} + \phi^{(3)})], \tag{30}$$
$$T_5^{(3)} = \mathrm{i}k^{(3)}c_{44}^{(V)}|R^{(3)}|(u_{zo}^{(3)}\cos\theta^{(3)} + u_{xo}^{(3)}\sin\theta^{(3)})\exp[\mathrm{i}(\omega t - k^{(3)}x\sin\theta^{(3)} - k^{(3)}z\cos\theta^{(3)} + \phi^{(3)})]. \tag{31}$$

From Eqs. (25)–(31) the z-components of power density fluxes are given by

$$P_z^{(0)} = \frac{1}{2}\omega k^{(0)}|R^{(0)}|^2[c_{44}^{(V)}\cos\theta^{(0)}(u_{xo}^{(0)})^2 + u_{xo}^{(0)}u_{zo}^{(0)}(c_{13}^{(V)} + c_{44}^{(V)})\sin\theta^{(0)} + c_{33}^{(V)}\cos\theta^{(0)}(u_{zo}^{(0)})^2], \tag{32}$$
$$P_z^{(1)} = \frac{1}{2}\omega k^{(1)}|R^{(1)}|^2[c_{44}^{(V)}\cos\theta^{(1)}(u_{xo}^{(1)})^2 + u_{xo}^{(1)}u_{zo}^{(1)}(c_{13}^{(V)} + c_{44}^{(V)})\sin\theta^{(1)} + c_{33}^{(V)}\cos\theta^{(1)}(u_{zo}^{(1)})^2], \tag{33}$$
$$P_z^{(3)} = \frac{1}{2}\omega k^{(3)}|R^{(3)}|^2[c_{44}^{(V)}\cos\theta^{(3)}(u_{zo}^{(3)})^2 + u_{xo}^{(3)}u_{zo}^{(3)}(c_{13}^{(V)} + c_{44}^{(V)})\sin\theta^{(3)} + c_{33}^{(V)}\cos\theta^{(3)}(u_{xo}^{(3)})^2]. \tag{34}$$

For the refracted P- and SV-waves propagating on the x–z plane within TTI medium, Eq. (22) can be written explicitly

$$\begin{pmatrix} T_1^{(m)} \\ T_2^{(m)} \\ T_3^{(m)} \\ T_4^{(m)} \\ T_5^{(m)} \\ T_6^{(m)} \end{pmatrix} = \begin{pmatrix} c_{11}^{(T)} & c_{12}^{(T)} & c_{13}^{(T)} & 0 & c_{15}^{(T)} & 0 \\ c_{12}^{(T)} & c_{11}^{(T)} & c_{23}^{(T)} & 0 & c_{25}^{(T)} & 0 \\ c_{13}^{(T)} & c_{23}^{(T)} & c_{33}^{(T)} & 0 & c_{35}^{(T)} & 0 \\ 0 & 0 & 0 & c_{44}^{(T)} & 0 & c_{46}^{(T)} \\ c_{15}^{(T)} & c_{25}^{(T)} & c_{35}^{(T)} & 0 & c_{55}^{(T)} & 0 \\ 0 & 0 & 0 & c_{46}^{(T)} & 0 & c_{66}^{(T)} \end{pmatrix} \begin{pmatrix} \partial/\partial x & 0 & 0 \\ 0 & 0 & 0 \\ 0 & 0 & \partial/\partial z \\ 0 & \partial/\partial z & 0 \\ \partial/\partial z & 0 & \partial/\partial x \\ 0 & \partial/\partial x & 0 \end{pmatrix} \begin{pmatrix} S_x^{(m)} \\ 0 \\ S_z^{(m)} \end{pmatrix}$$
$$= \begin{pmatrix} \left(c_{11}^{(T)}\dfrac{\partial}{\partial x} + c_{15}^{(T)}\dfrac{\partial}{\partial z}\right)S_x^{(m)} + \left(c_{13}^{(T)}\dfrac{\partial}{\partial z} + c_{15}^{(T)}\dfrac{\partial}{\partial x}\right)S_z^{(m)} \\ \left(c_{12}^{(T)}\dfrac{\partial}{\partial x} + c_{25}^{(T)}\dfrac{\partial}{\partial z}\right)S_x^{(m)} + \left(c_{23}^{(T)}\dfrac{\partial}{\partial z} + c_{25}^{(T)}\dfrac{\partial}{\partial x}\right)S_z^{(m)} \\ \left(c_{13}^{(T)}\dfrac{\partial}{\partial x} + c_{35}^{(T)}\dfrac{\partial}{\partial z}\right)S_x^{(m)} + \left(c_{33}^{(T)}\dfrac{\partial}{\partial z} + c_{35}^{(T)}\dfrac{\partial}{\partial x}\right)S_z^{(m)} \\ 0 \\ \left(c_{15}^{(T)}\dfrac{\partial}{\partial x} + c_{55}^{(T)}\dfrac{\partial}{\partial z}\right)S_x^{(m)} + \left(c_{35}^{(T)}\dfrac{\partial}{\partial z} + c_{55}^{(T)}\dfrac{\partial}{\partial x}\right)S_z^{(m)} \\ 0 \end{pmatrix}, \tag{35}$$

where $\{m\} = \{2, 4\}$ are for the refracted P- and SV-waves; $S_x^{(m)}$ and $S_z^{(m)}$ are x- and z-components. So, we have stress related to the z-components of density flux for refracted P- and SV-waves

$$T_3^{(2)} = \mathrm{i}k^{(2)}|R^{(2)}|[(-c_{13}^{(V)}\sin\theta^{(2)} + c_{35}^{(V)}\cos\theta^{(2)})u_{xo}^{(2)} - (c_{33}^{(V)}\cos\theta^{(2)} - c_{35}^{(V)}\cos\theta^{(2)})u_{zo}^{(2)}] \times \exp[\mathrm{i}(\omega t - k^{(2)}x\sin\theta^{(2)} + k^{(2)}z\cos\theta^{(2)} + \phi^{(2)}], \quad (36)$$

$$T_5^{(2)} = -\mathrm{i}k^{(2)}|R^{(2)}|[u_{xo}^{(2)}(-c_{15}^{(V)}\sin\theta^{(2)} + c_{55}^{(V)}\cos\theta^{(2)}) - u_{zo}^{(2)}(c_{35}^{(V)}\cos\theta^{(2)} - c_{55}^{(V)}\sin\theta^{(3)})] \times \exp[\mathrm{i}(\omega t - k^{(2)}x\sin\theta^{(2)} + k^{(2)}z\cos\theta^{(2)} + \phi^{(2)}], \quad (37)$$

$$T_3^{(4)} = \mathrm{i}k^{(4)}|R^{(4)}|[u_{zo}^{(4)}(c_{13}^{(V)}\sin\theta^{(4)} - c_{35}^{(V)}\cos\theta^{(4)}) + u_{xo}^{(2)}(c_{33}^{(V)}\cos\theta^{(4)} - c_{35}^{(V)}\sin\theta^{(4)})] \times \exp[\mathrm{i}(\omega t - k^{(4)}x\sin\theta^{(4)} + k^{(4)}z\cos\theta^{(4)} + \phi^{(4)}], \quad (38)$$

$$T_5^{(4)} = \mathrm{i}k^{(4)}|R^{(4)}|[u_{zo}^{(4)}(c_{15}^{(V)}\sin\theta^{(4)} - c_{55}^{(V)}\cos\theta^{(4)}) + u_{xo}^{(4)}(c_{35}^{(V)}\cos\theta^{(4)} - c_{55}^{(V)}\sin\theta^{(4)})] \times \exp[\mathrm{i}(\omega t - k^{(4)}x\sin\theta^{(4)} + k^{(4)}z\cos\theta^{(4)} + \phi^{(4)}]. \quad (39)$$

From Eqs. (25) and (35)–(39), the z-components of power density fluxes of the refracted P- and SV-waves can be written by

$$P_z^{(2)} = -\frac{1}{2}\omega k^{(2)}|R^{(2)}|^2\{(u_{xo}^{(2)})^2(-c_{15}^{(V)}\sin\theta^{(2)} + c_{55}^{(V)}\cos\theta^{(2)}) - u_{xo}^{(2)}u_{zo}^{(2)}[(c_{33}^{(V)} + c_{35}^{(V)})\cos\theta^{(2)} + (c_{13}^{(V)} + c_{55}^{(V)})\sin\theta^{(2)}] - (u_{zo}^{(2)})^2(c_{33}^{(V)}\cos\theta^{(2)} - c_{35}^{(V)}\sin\theta^{(2)})\}, \quad (40)$$

$$P_z^{(4)} = -\frac{1}{2}\omega k^{(4)}|R^{(4)}|^2\{(u_{zo}^{(4)})^2(c_{55}^{(V)}\cos\theta^{(4)} - c_{15}^{(V)}\sin\theta^{(4)}) + [(c_{13}^{(V)} + c_{55}^{(V)})\sin\theta^{(4)} - 2c_{35}^{(V)}\cos\theta^{(4)})]u_{xo}^{(4)}u_{zo}^{(4)} + (u_{xo}^{(4)})^2(c_{35}^{(V)}\sin\theta^{(4)} - c_{33}^{(V)}\cos\theta^{(4)})\}. \quad (41)$$

2.3 Determination of polarization coefficients at VTI-TTI interface

The polarization coefficients can be analyzed from Eq. (11) which yields

$$\frac{u_z^{(m)}}{u_x^{(m)}} = -\frac{\Gamma_{11}^{(m)} - (v_{1,2}^{(m)})^2}{\Gamma_{13}^{(m)}}, \quad (42)$$

$$\frac{u_x^{(m)}}{u_z^{(m)}} = -\frac{\Gamma_{33}^{(m)} - (v_{1,2}^{(m)})^2}{\Gamma_{13}^{(m)}}. \quad (43)$$

Combining Eqs. (42) and (43) with the normalized condition $u_x^{(m)}[u_x^{(m)}]^* + u_z^{(m)}[u_z^{(m)}]^* = 1$, we have

$$(u_x^{(m)})^* u_z^{(m)} = -\frac{\Gamma_{13}^{(m)}(\Gamma_{13}^{(m)})^*}{(\Gamma_{13}^{(m)})^*[\Gamma_{33}^{(m)} - (v_{1,2}^{(m)})^2] + \Gamma_{13}^{(m)}[\Gamma_{11}^{(m)} - (v_{1,2}^{(m)})^2]^*}, \quad (44)$$

$$u_x^{(m)}(u_z^{(m)})^* = -\frac{\Gamma_{13}^{(m)}(\Gamma_{13}^{(m)})^*}{\Gamma_{13}^{(m)}[\Gamma_{33}^{(m)} - (v_{1,2}^{(m)})^2]^* + (\Gamma_{13}^{(m)})^*[\Gamma_{11}^{(m)} - (v_{1,2}^{(m)})^2]}, \quad (45)$$

where the superscription * signifies complex conjugate. In the combination of Eq. (43) and Eq. (45), we obtain

$$u_x^{(m)}[u_x^{(m)}]^* = |u_x^{(m)}|^2 = u_x^{(m)}[u_z^{(m)}]^*\left[\frac{u_x^{(m)}}{u_z^{(m)}}\right]^* = \frac{\Gamma_{13}^{(m)}[\Gamma_{13}^{(m)}]^*}{\Gamma_{13}^{(m)}[\Gamma_{13}^{(m)}]^* + \{\Gamma_{11}^{(m)} - [v_{1,2}^{(m)}]^2\}\{\Gamma_{11}^{(m)} - [v_{1,2}^{(m)}]^2\}^*}. \quad (46)$$

Similarly, the combination of Eqs. (42) and (44) yields

$$u_z^{(m)}[u_z^{(m)}]^* = |u_z^{(m)}|^2 = [u_x^{(m)}]^* u_z^{(m)}\left[\frac{u_z^{(m)}}{u_x^{(m)}}\right]^* = \frac{\Gamma_{13}^{(m)}[\Gamma_{13}^{(m)}]^*}{\Gamma_{13}^{(m)}[\Gamma_{13}^{(m)}]^* + \{\Gamma_{33}^{(m)} - [v_{1,2}^{(m)}]^2\}\{\Gamma_{33}^{(m)} - [v_{1,2}^{(m)}]^2\}^*}. \quad (47)$$

Now, we can summarize our understanding of the polarization coefficients and classify them based on the location of the incidence angles.

(i) In the pre-incident critical-angle region, all waves are homogeneous and the polarization coefficients are real numbers (not complex). Consequently, $b_1^{(m)}$ and $b_3^{(m)}$ in Eq. (10) are zero. Then, we have from Eqs. (46) and (47)

$$u_x^{(m)} = a_1^{(m)} = \sqrt{\frac{\Gamma_{33}^{(m)} - (v_{1,2}^{(m)})^2}{\Gamma_{11}^{(m)} + \Gamma_{33}^{(m)} - 2(v_{1,2}^{(m)})^2}}, \quad (48)$$

$$u_z^{(m)} = a_3^{(m)} = \sqrt{\frac{\Gamma_{11}^{(m)} - (v_{1,2}^{(m)})^2}{\Gamma_{11}^{(m)} + \Gamma_{33}^{(m)} - 2(v_{1,2}^{(m)})^2}}. \quad (49)$$

(ii) In the post-incident critical-angle region, the polarization coefficients of incident P-wave are again purely

real number as in (i), and again we have Eqs. (48) and (49). However, the reflected P- and SV-waves and the refracted SV-wave create a phase shift from incident P-wave. Their reflection and refraction coefficients are complex numbers. So, the polarization coefficients are written as

$$\begin{aligned} u_x^{(m)} &= |u_x^{(m)}| \exp[\mathrm{i}\phi^{(m)}] = a_1^{(m)} + \mathrm{i}b_1^{(m)} \\ &= (\cos\phi^{(m)} + \mathrm{i}\sin\phi^{(m)}) \sqrt{\frac{\Gamma_{13}^{(m)}[\Gamma_{13}^{(m)}]^*}{\Gamma_{13}^{(m)}[\Gamma_{13}^{(m)}]^* + \{\Gamma_{11}^{(m)} - [v_{1,2}^{(m)}]^2\}\{\Gamma_{11}^{(m)} - [v_{1,2}^{(m)}]^2\}^*}}, \end{aligned} \tag{50}$$

$$\begin{aligned} u_z^{(m)} &= |u_z^{(m)}| \exp[\mathrm{i}\phi^{(m)}] = a_3^{(m)} + \mathrm{i}b_3^{(m)} \\ &= (\cos\phi^{(m)} + \mathrm{i}\sin\phi^{(m)}) \sqrt{\frac{\Gamma_{13}^{(m)}[\Gamma_{13}^{(m)}]^*}{\Gamma_{13}^{(m)}[\Gamma_{13}^{(m)}]^* + \{\Gamma_{33}^{(m)} - [v_{1,2}^{(m)}]^2\}\{\Gamma_{33}^{(m)} - [v_{1,2}^{(m)}]^2\}^*}}, \end{aligned} \tag{51}$$

where the superscript $\{m\} = \{1, 3, 4\}$.

(iii) In the post-incident critical-angle region, the refracted P-wave becomes inhomogeneous. The real part of the z-component of the power density flux is zero definite. From Eq. (10) we have $u_x^{(m)} = a_1^{(m)} + \mathrm{i}b_1^{(m)}$ and $u_z^{(m)} = a_3^{(m)} + \mathrm{i}b_3^{(m)}$. Substitution of these relations into Eq. (40) leads to

$$a_1^{(2)} a_3^{(2)} + b_1^{(2)} b_3^{(2)} = 0. \tag{52}$$

Additionally, from Eq. (52), we obtain

$$\begin{aligned} u_x^{(2)}[u_z^{(2)}]^* &= (a_1^{(2)} + \mathrm{i}b_1^{(2)})(a_3^{(2)} - \mathrm{i}b_3^{(2)}) \\ &= \mathrm{i}(b_1^{(2)} a_3^{(2)} - a_1^{(2)} b_3^{(2)}) \end{aligned} \tag{53}$$

or

$$\begin{aligned} u_z^{(2)}[u_x^{(2)}]^* &= (a_1^{(2)} - \mathrm{i}b_1^{(2)})(a_3^{(2)} + \mathrm{i}b_3^{(2)}) \\ &= -\mathrm{i}(b_1^{(2)} a_3^{(2)} - a_1^{(2)} b_3^{(2)}). \end{aligned} \tag{54}$$

Eqs. (53) and (54) guarantee that when the x-component ($u_x^{(m)}$) is real, the z-component ($u_z^{(m)}$) must be purely imaginary and vice versa. Then, the polarization coefficients of an inhomogeneous refracted P-waves can be written as

$$u_x^{(2)} = \sqrt{\frac{|\Gamma_{13}^{(2)}[\Gamma_{33}^{(2)} - (v_{1,2}^{(2)})^2]|}{|(\Gamma_{13}^{(2)})^*[\Gamma_{33}^{(2)} - (v_{1,2}^{(2)})^2] + \Gamma_{13}^{(2)}[\Gamma_{11}^{(2)} - (v_{1,2}^{(2)})^2]|}}, \tag{55}$$

$$u_z^{(2)} = \mathrm{i}\sqrt{\frac{|\Gamma_{13}^{(2)}(\Gamma_{33}^{(2)} - (v_{1,2}^{(2)})^2)|}{|(\Gamma_{13}^{(2)})^*(\Gamma_{33}^{(2)} - (v_{1,2}^{(2)})^2) + \Gamma_{13}^{(2)}(\Gamma_{11}^{(2)} - (v_{1,2}^{(2)})^2)|}}, \tag{56}$$

or

$$u_x^{(2)} = \mathrm{i}\sqrt{\frac{|\Gamma_{13}^{(2)}[\Gamma_{33}^{(2)} - (v_{1,2}^{(2)})^2]|}{|(\Gamma_{13}^{(2)})^*[\Gamma_{33}^{(2)} - (v_{1,2}^{(2)})^2] + \Gamma_{13}^{(2)}[\Gamma_{11}^{(2)} - (v_{1,2}^{(2)})^2]|}}, \tag{57}$$

$$u_z^{(2)} = \sqrt{\frac{|\Gamma_{13}^{(2)}[\Gamma_{33}^{(2)} - (v_{1,2}^{(2)})^2]|}{|(\Gamma_{13}^{(2)})^*[\Gamma_{33}^{(2)} - (v_{1,2}^{(2)})^2] + \Gamma_{13}^{(2)}[\Gamma_{11}^{(2)} - (v_{1,2}^{(2)})^2]|}}. \tag{58}$$

The selection of the polarization coefficients of an inhomogeneously refracted P-wave from Eqs. (55)–(58) has to be determined by the rotational direction of its elliptical polarization [36–39].

2.4 A high-order polynomial for solving reflection and refraction angles

Consider an incidence of P-wave propagating from VTI to TTI with an incident-angle θ. At the VTI-TTI media interface, Snell's law provides the following relationships

$$\mathrm{const}_V(\theta) = \left[\frac{\sin\theta^{(m)}}{v_{1,2}^{(m)}}\right]^2, \tag{59}$$

$$\mathrm{const}^{(V)}(\theta) = \left[\frac{\sin\theta}{v_1^{(0)}(\theta)}\right]^2 = \frac{2\sin^2\theta}{A_4^{(V)}\sin^2\theta + A_5^{(V)} + Q^{(V)}(\theta)}. \tag{60}$$

Inside VTI incidence medium, a combination of Eqs. (15), (59), and (60) leads to a fourth-order polynomial with respect to reflection angle for the reflected P- and SV-waves [33, 34]

$$B_1^{(1,3)}(\theta)\sin^4\theta^{(1,3)} + B_3^{(1,3)}(\theta)\sin^2\theta^{(1,3)} + B_5^{(1,3)} = 0, \tag{61}$$

where

$$B_1^{(1,3)}(\theta) = A_1^{(V)} - 2(A_1^{(V)}A_2^{(V)} + 2[A_3^{(V)}]^2) + A_2^{(V)} - [K^{(V)}(\theta)]^2,$$

$$B_3^{(1,3)}(\theta) = 2[A_1^{(V)}A_2^{(V)} + [A_3^{(V)}]^2 - [A_2^{(V)}]^2 + A_5^{(V)}K^{(V)}(\theta)],$$

$$B_5^{(1,3)} = A_2^{(V)} - [A_5^{(V)}]^2,$$

and

$$K^{(V)}(\theta) = 2/\mathrm{const}^{(V)}(\theta) - A_4^{(V)}.$$

Inside TTI refraction medium, a combination of Eqs. (20), (59), and (60) yields in an eighth-order polynomial for solving refraction angle for refracted P- and SV-waves

$$f_1^{(2,4)}(\theta)\sin^8\theta^{(2,4)}+f_2^{(2,4)}(\theta)\sin^6\theta^{(2,4)}+f_3^{(2,4)}(\theta)\sin^4\theta^{(2,4)} + f_4^{(2,4)}(\theta)\sin^2\theta^{(2,4)}+f_5^{(2,4)}=0, \tag{62}$$

where

$f_1^{(2,4)}(\theta)=[d_1^2+d_2^2]^2-8d_1d_3-8d_2d_3+16d_3^2+4d_4^2-8d_4d_5+4d_5^2$,
$f_2^{(2,4)}=4(-d_1d_2-d_2^2+2d_1d_3+6d_2d_3-8d_3^2-d_4^2+4d_4d_5-3d_5^2)$,
$f_3^{(2,4)}(\theta)=2(d_1d_2+3d_2^2-12d_2d_3+8d_3^2-4d_4d_5+6d_5)$, $f_4^{(2,4)}(\theta)=4(-d_2^2+2d_2d_3-d_5^2)$,
$f_5^{(2,4)}=d_2^2$, $d_1=b_1-c_4^2$, $d_2=b_2-c_3^2$, $d_3=b_3-c_2^2+c_3c_4/2$, $d_4=b_4+2c_2c_4$,
$d_5=b_5-2c_2c_3$ and $c_4=\mathrm{const}^{(V)}(\theta)/2-c_1$.

2.5 Matrix equation of reflection and refraction coefficients

From Eqs. (5)–(9) and (22), in considerations of the boundary conditions for continuity of the normal stress components and the components of particle displacement, we obtain a matrix equation for reflection and refraction coefficients, connecting to incident-angle, polarization coefficient, and physical parameters of the media

$$\begin{pmatrix} M_{11} & M_{12} & M_{13} & M_{14} \\ M_{21} & M_{22} & M_{23} & M_{24} \\ M_{31} & M_{32} & M_{33} & M_{34} \\ M_{41} & M_{42} & M_{43} & M_{44} \end{pmatrix} \begin{pmatrix} R_{pp} \\ R_{ps} \\ T_{pp} \\ T_{ps} \end{pmatrix} = \begin{pmatrix} N_1 \\ N_2 \\ N_3 \\ N_4 \end{pmatrix}, \tag{63}$$

where,

$N_1=-k^{(0)}(c_{13}^{(v)}u_x^{(0)}\sin\theta^{(0)}+c_{33}^{(v)}u_z^{(0)}\cos\theta^{(0)})$, $N_2=k^{(0)}c_{44}^{(v)}(u_x^{(0)}\cos\theta^{(0)}+u_z^{(0)}\sin\theta^{(0)})$,
$N_3=-u_x^{(0)}$, $N_4=u_z^{(0)}$, $M_{11}=k^{(1)}(c_{13}^{(v)}u_x^{(1)}\sin\theta^{(1)}+c_{33}^{(v)}u_z^{(1)}\cos\theta^{(1)})$,
$M_{12}=-k^{(3)}(c_{13}^{(v)}u_z^{(3)}\sin\theta^{(3)}+c_{33}^{(0)}u_x^{(3)}\cos\theta^{(3)})$,
$M_{13}=-k^{(2)}(c_{13}^{(T)}u_x^{(2)}\sin\theta^{(2)}+c_{33}^{(T)}u_z^{(2)}\cos\theta^{(2)})+k^{(2)}c_{35}^{(T)}(u_x^{(2)}\cos\theta^{(2)}+u_z^{(2)}\sin\theta^{(2)})$,
$M_{14}=-k^{(4)}(c_{13}^{(T)}u_z^{(4)}\sin\theta^{(4)}-c_{33}^{(T)}u_x^{(4)}\cos\theta^{(4)})+k^{(4)}c_{35}^{(T)}(u_z^{(4)}\cos\theta^{(4)}-u_x^{(4)}\sin\theta^{(4)})$,
$M_{21}=k^{(1)}c_{44}^{(0)}(u_x^{(1)}\cos\theta^{(1)}+u_z^{(1)}\sin\theta^{(1)})$, $M_{22}=-k^{(3)}c_{44}^{(0)}(u_z^{(3)}\cos\theta^{(3)}+u_x^{(3)}\sin\theta^{(3)})$,
$M_{23}=-k^{(2)}(c_{15}^{(T)}u_x^{(2)}\sin\theta^{(2)}+c_{35}^{(T)}u_z^{(2)}\cos\theta^{(2)})+k^{(2)}c_{55}^{(T)}(u_x^{(2)}\cos\theta^{(2)}+u_z^{(2)}\sin\theta^{(2)})$,
$M_{24}=-k^{(4)}(c_{15}^{(T)}u_z^{(4)}\sin\theta^{(4)}-c_{35}^{(T)}u_x^{(4)}\cos\theta^{(4)})+k^{(4)}c_{55}^{(T)}(u_z^{(4)}\cos\theta^{(4)}-u_x^{(4)}\sin\theta^{(4)})$,

and $M_{31}=u_x^{(1)}$, $M_{32}=-u_z^{(3)}$, $M_{33}=-u_x^{(2)}$, $M_{34}=-u_z^{(4)}$, $M_{41}=u_z^{(1)}$, $M_{42}=-u_x^{(3)}$, $M_{43}=u_z^{(2)}$ and $M_{44}=-u_x^{(4)}$.

3 Calculation and discussion

For VTI-TTI media interface with a given set of anisotropic and physical parameters, the coefficients, i.e., $B_1^{(1,3)}(\theta)$, $B_3^{(1,3)}(\theta)$, $f_1^{(2,4)}(\theta)$, $f_2^{(2,4)}(\theta)$, $f_3^{(2,4)}(\theta)$ and $f_4^{(2,4)}(\theta)$, in Eqs. (61) and (62) are functions of the incident angle θ; while the coefficients $B_5^{(1,3)}$ and $f_5^{(2,4)}$ are independent of incident angle θ. As an example, we select a model with one incident critical-angle corresponding to refracted P-wave, which is a modified Daley-Hron system model [27, 28, 34]. The system parameters are shown in Table 1. Discussions on cases without incident critical-angle are similar to that of pre-critical-angle incidence for this modified system.

The anisotropic parameters are related to rock stiffness matrix elements by [23]

$$c_{13}=\rho\sqrt{[\delta^*\alpha^4+(\alpha^2-\beta^2)][(\varepsilon+1)\alpha^2-\beta^2]}-\rho\beta^2, \tag{64a}$$
$$c_{33}=\rho\alpha^2, \tag{64b}$$
$$c_{11}=(2\varepsilon+1)\rho\alpha^2, \tag{64c}$$
$$c_{44}=\rho\beta^2, \tag{64d}$$
$$c_{66}=(2\gamma+1)\rho\beta, \tag{64e}$$

where α and β are the phase velocities of P-and SV-waves in symmetric axis direction of the VTI medium; ε, δ^* and γ are the anisotropic rock parameters.

From Eqs. (15) and (20), the slowness curves have been calculated and shown in Fig. 3. It shows that the slowness of P-wave in incidence (VTI) medium is larger than that of P-wave and smaller than that of SV-wave in the refraction

Table 1 Physical and anisotropic parameters of the model system: MDMI stands for incidence medium and MDMR stands for refraction medium.

Medium	α (m/s)	β (m/s)	ε	δ^*	γ	ρ (g/cm^3)
MDMI	2310	1330	0.2132	0.0000	0.0000	2.040
MDMR	3060	1770	0.2132	0.0000	0.0000	2.210

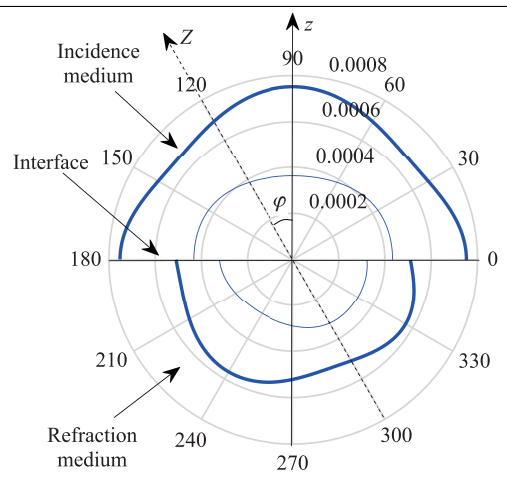


Fig. 3 The calculated slowness: the upside of the interface is VTI (incidence) medium and the downside is TTI (refraction) medium. The thin curve shows the slowness of P-wave and thick curves are that of SV-wave.

(TTI) medium. This is a case where there is an incident critical-angle ($\theta_c^{(2)}$) corresponding to the refracted P-wave.

The calculated values of $\sin\theta^{(m)}/v^{(m)}(\theta^{(m)})$ versus θ are shown in Fig. 4. Curve 0 is the relationship of $\sin\theta/v^{(0)}(\theta)$ versus θ; Curves 1, 2, 3 and 4 are those of $\sin\theta^{(1)}/v^{(1)}(\theta^{(1)})$, $\sin\theta^{(2)}/v^{(2)}(\theta^{(2)})$, $\sin\theta^{(3)}/v^{(3)}(\theta^{(3)})$ and $\sin\theta^{(4)}/v^{(4)}(\theta^{(4)})$ versus θ. These five curves (0–4) are identical which means that these calculated results abide by Snell's law. This provides us an added confidence in the established fourth-order and eighth-order polynomials for calculations of reflection and refraction angles.

3.1 Calculation of incident critical-angle corresponding to refraction P-wave

Figure 3 shows that there is an incident critical-angle corresponding to refraction P-wave for this VTI-TTI media interface. The combination of Eqs. (15), (16), (20) and (21) with Snell's law leads to an equation for incident critical-angle ($\theta_c^{(2)}$)

$$l_1\sin^4\theta_c^{(2)} + l_3\sin^2\theta_c^{(2)} + l_5 = 0, \tag{65}$$

where $A_6^{(V)} = A_1^{(V)} - A_2^{(V)} + A_7^{(V)}$, $A_7 = 4[A_3^{(V)}]^2$, $D = c_1 + \sqrt{b_1}$, $e = D - A_4^{(V)}$, $l_1 = e^2 + A_7^{(V)}$, $l_3 = -(2eA_5^{(V)} + A_6^{(V)})$ and $l_5 = [A_5^{(V)}]^2 - A_2^{(V)}$.

In terms of Eq. (65), we have calculated $\theta_c^{(2)}$ versus $\varepsilon^{(1)}$, $\delta^{*(1)}$, $\varepsilon^{(2)}$, $\delta^{*(2)}$ and φ, respectively, as shown in Fig. 5. These calculated results show that for $\varphi = 30°$, $\theta_c^{(2)}$ increases with increasing anisotropic parameters of the incidence medium ($\varepsilon^{(1)}$ and $\delta^{*(1)}$). Meanwhile, the critical angle ($\theta_c^{(2)}$) decreases with increasing anisotropic parameters of refraction medium ($\varepsilon^{(2)}$ and $\delta^{*(2)}$). The effect of one parameter ($\varepsilon^{(2)}$) on the critical angle ($\theta_c^{(2)}$) is greater than that of another ($\delta^{*(2)}$).

Figure 5(c) shows that $\theta_c^{(2)}$ increases with increasing φ. At $\varphi = 0°$, the value of the incident critical-angle from Eq. (65) is equal to that calculated by using the VTI-VTI media interface model [33, 34], i.e., the value represented by sign "five-pointed star" is the same as that of the curve at $\varphi = 0°$. This can be used as an added check for VTI-TTI interface model established in this paper.

Because the coefficients l_1, l_3, and l_5 in Eq. (65) are not related to incident-angle, the incident critical-angle $\theta_c^{(2)}$ is not related to incident-angle. It is purely determined by the physical and anisotropic parameters of the incidence and refraction media and the tilt-angle of the refraction medium. The larger the anisotropic parameter and the value of φ are, the greater the variation of $\theta_c^{(2)}$ is.

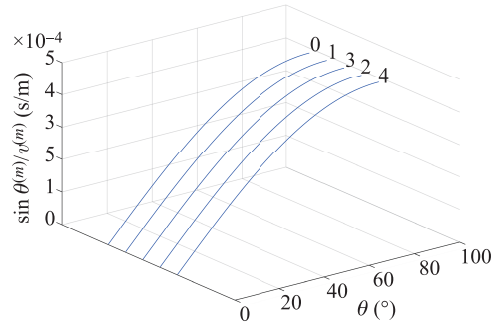


Fig. 4 Relationships of $\sin\theta^{(m)}/v^{(m)}(\theta^{(m)})$ vs. θ.

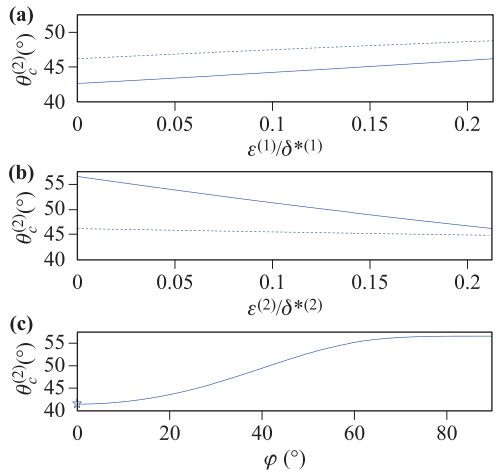


Fig. 5 Reationships of $\theta_c^{(2)}$ vs. $\varepsilon^{(1)}$, $\delta^{*(1)}$, $\varepsilon^{(2)}$, and $\delta^{*(2)}$ at $\varphi = 30°$ and $\theta_c^{(2)}$ vs. φ: **(a)** $\theta_c^{(2)}$ vs. $\varepsilon^{(1)}$ and $\delta^{*(1)}$, where solid-curve is for $\varepsilon^{(1)}$ and dashed-curve is for $\delta^{*(1)}$; **(b)** $\theta_c^{(2)}$ vs. $\varepsilon^{(2)}$ and $\delta^{*(2)}$, where solid-curve is for $\varepsilon^{(2)}$ and dashed-curve is for $\delta^{*(2)}$; **(c)** $\theta_c^{(2)}$ vs. φ, and the sign "five-pointed star" is the value of incident critical-angle calculated by using VTI-VTI media interface model.

3.2 The effects of anisotropic parameters of media on reflection and refraction coefficients

At $\varphi = 30°$, we have calculated the reflection and refraction coefficients from Eq. (63), as shown in Figs. 6–9, which provides the following insightful information.

(i) The anisotropy of incidence/refraction media may cause the amplitude and phase of reflection and refraction coefficients to change for any given incident-angle. The effects of anisotropy from the refraction medium are greater than that of the incidence medium.

(ii) The variations near $\theta_c^{(2)}$ and in the post-incident critical-angle region are more significant than that of a smaller incident angle.

(iii) In the pre-critical incident-angle region, the phase angle of the reflection and refraction coefficients can be either 0° or 180° only. The phase change from incident P-wave is either in the same phase or in the anti-phase; $R^{(1)}$ and $R^{(2)}$ are positive real number at phase angles equal to 0°; $R^{(3)}$ and $R^{(4)}$ are negative real numbers at phase angles equal to 180°.

(iv) At $\theta = \theta_c^{(2)}$, the reflection and refraction coefficients are not continuous.

(v) In the post-critical incident angle region, the reflection and refraction coefficients are complex numbers and the phase angles create variation. We have observed an interesting phenomenon: for the induced homogenous waves, i.e., reflected P-wave, reflected SV-wave and refracted SV-wave, the corresponding phase angles are positive. For the induced inhomogeneous waves, i.e., the refracted P-wave, the corresponding phase angle can be either positive or negative.

In the post-critical incident angle region, the induced waves will yield a phase shift relative to the incidence of P-wave. Mapping this phase shift to time-domain yields a transition-time relative to the incident P-wave; while mapping it to space domain yields a lateral-displacement on the interface. This has actually been predicted by Zhu *et al.* [21] and Fa *et al.* [22] in acoustic-logging. They pointed out that the first arrival of measured acoustic signal may be reflected P-wave induced on borehole-wall for the case of post-critical-angle incidence. Therefore, accurate phase information of $R^{(1)}$ is important not only to the accurate time-depth conversion of seismic exploration data but also to the accurate measurement of the propagation speed of P-wave in the medium around borehole for acoustic-logging. While the accurate amplitude information of $R^{(1)}$ is important for AVO analysis of seismic exploration data.

3.3 The effects of tilt-angle of refraction medium on reflection and refraction coefficients

Considering the tilt-angle (φ) of refraction medium we have calculated the reflection and refraction coefficients, shown in Fig. 10. Apparently, φ exerts an even greater

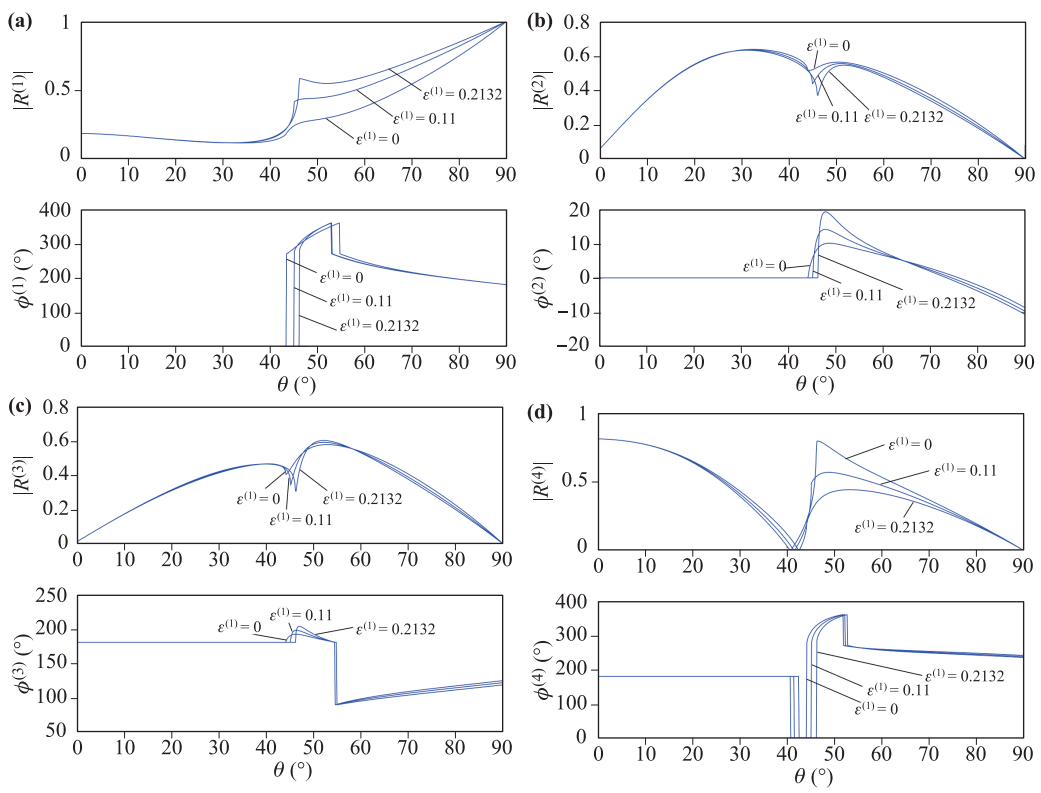


Fig. 6 $R^{(1)}$, $R^{(2)}$, $R^{(3)}$, and $R^{(4)}$ vs. θ for several different values of $\varepsilon^{(1)}$, where upper chart is modulus and lower chart is its corresponding phase: **(a)** The modulus and phase of $R^{(1)}$; **(b)** those of $R^{(2)}$; **(c)** those of $R^{(3)}$; **(d)** those of $R^{(4)}$.

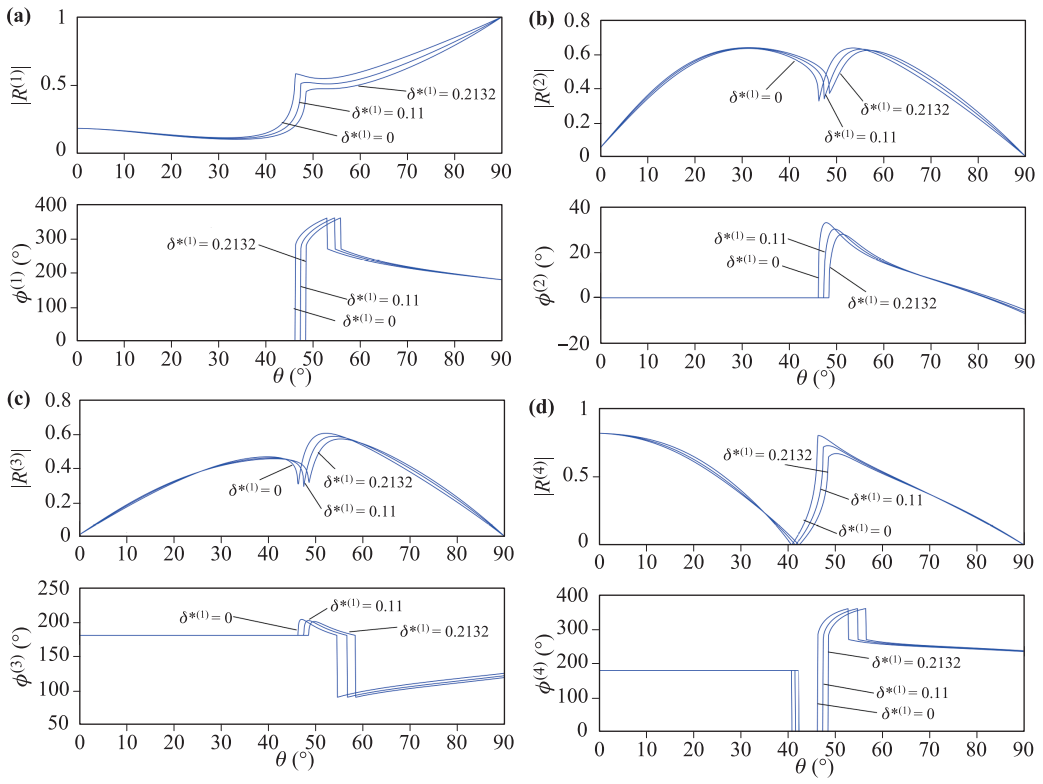


Fig. 7 $R^{(1)}$, $R^{(2)}$, $R^{(3)}$, and $R^{(4)}$ vs. θ for several different values of $\delta^{*(1)}$, where upper chart is modulus and lower chart is its corresponding phase: **(a)** The modulus and phase of $R^{(1)}$; **(b)** those of $R^{(2)}$; **(c)** those of $R^{(3)}$; **(d)** those of $R^{(4)}$.

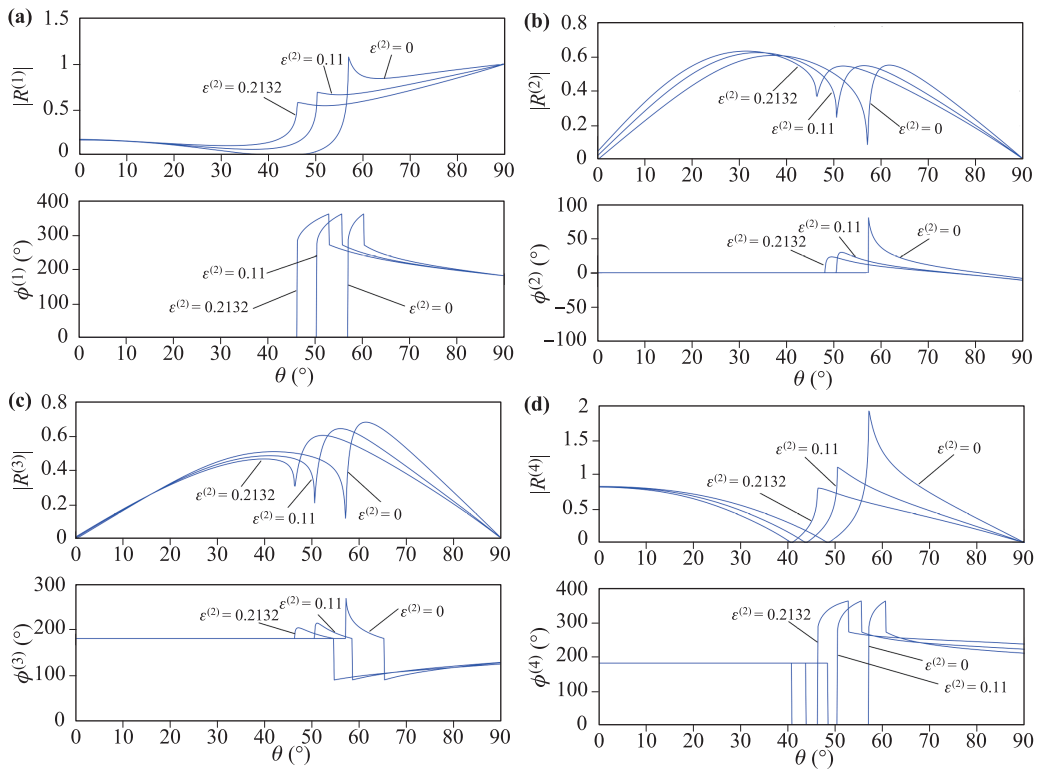


Fig. 8 $R^{(1)}$, $R^{(2)}$, $R^{(3)}$, and $R^{(4)}$ vs. θ for several different values of $\varepsilon^{(2)}$, where upper chart is modulus and lower chart is its corresponding phase: **(a)** The modulus and phase of $R^{(1)}$; **(b)** those of $R^{(2)}$; **(c)** those of $R^{(3)}$; **(d)** those of $R^{(4)}$.

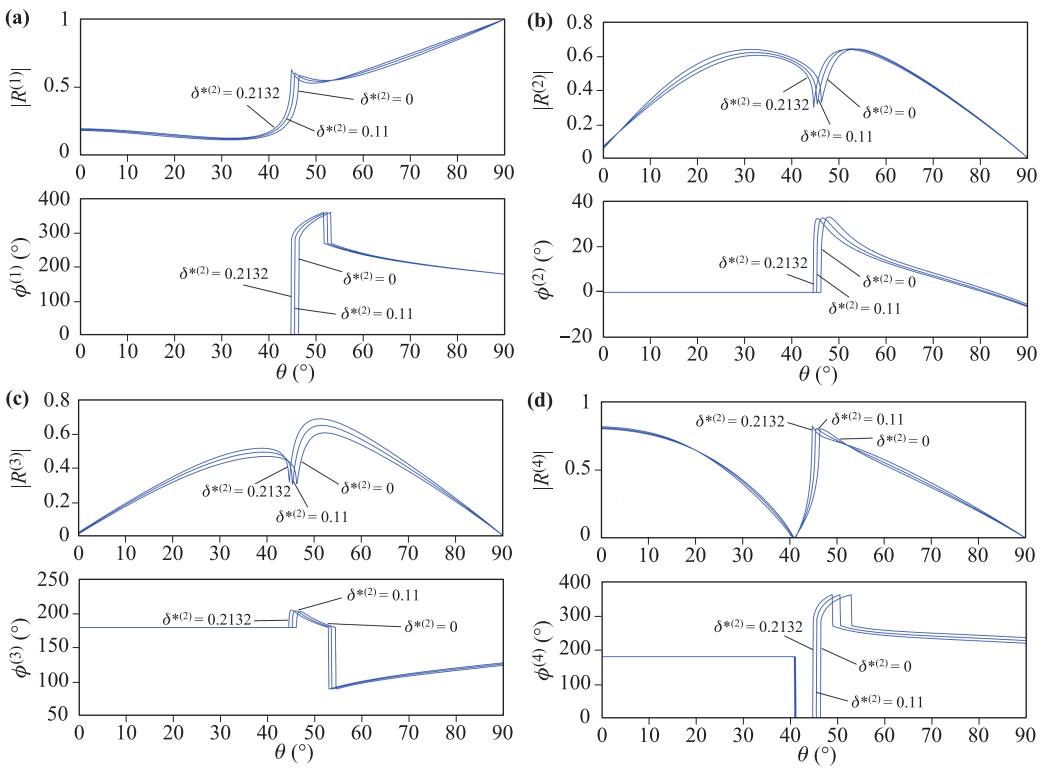


Fig. 9 $R^{(1)}$, $R^{(2)}$, $R^{(3)}$, and $R^{(4)}$ vs. θ for several different values of $\delta^{*(2)}$, where upper chart is modulus and lower chart is its corresponding phase: **(a)** The modulus and phase of $R^{(1)}$; **(b)** those of $R^{(2)}$; **(c)** those of $R^{(3)}$; **(d)** those of $R^{(4)}$.

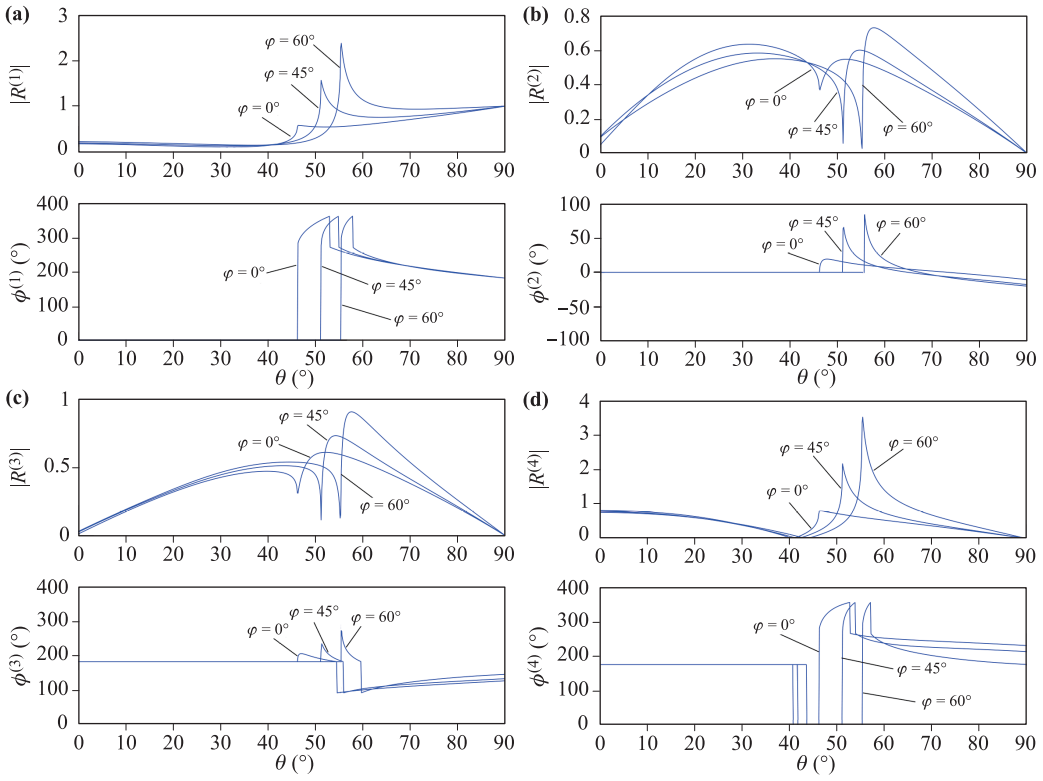


Fig. 10 $R^{(1)}$, $R^{(2)}$, $R^{(3)}$, and $R^{(4)}$ vs. θ for several different values of φ, where upper chart is a modulus and lower chart is the corresponding phase: **(a)** The modulus and phase of $R^{(1)}$, **(b)** those of $R^{(2)}$, **(c)** those of $R^{(3)}$, and **(d)** those of $R^{(4)}$.

influence on reflection and refraction coefficients than that of anisotropic parameters of the rock media.

3.4 The law of energy conservation

As an added confidence to our analysis of the reflection and refraction coefficients, we have analyzed the energy states at the interface. The law of energy conservation requires that z-component of power density flux of incident P-wave ($P_z^{(0)}$) equals the sum of z-component real-part of energy density fluxes from the waves induced at VTI-TTI interface.

The real-parts of z-components of energy density fluxes from the induced waves as a function of incident angle are calculated for several parameters and are shown in Figs. 11–15. The quantities of $|P_z^{(0)}|$ and $|\mathrm{Re}\{P_z^{(s)}\}|$ are calculated and are shown in Figs. 16–18. The three-dimensional charts shown in Figs. 16(a)–18(a) are rotated 90° clockwise to provide the two-dimensional views, as shown in Figs. 16(b)–18(b).

Figures 16 and 17 are the quantities for the different values of $\varepsilon^{(1)}$ and those for the different values of $\delta^{*(1)}$, respectively. It is noted that curves in Figs. 16 and 17 are different from each other. Using the parameters in Table 1, Fig. 18 shows the quantities for the different values of $\varepsilon^{(2)}$, of $\delta^{*(2)}$, and of φ. These three curves are identical and they stack together, one over others.

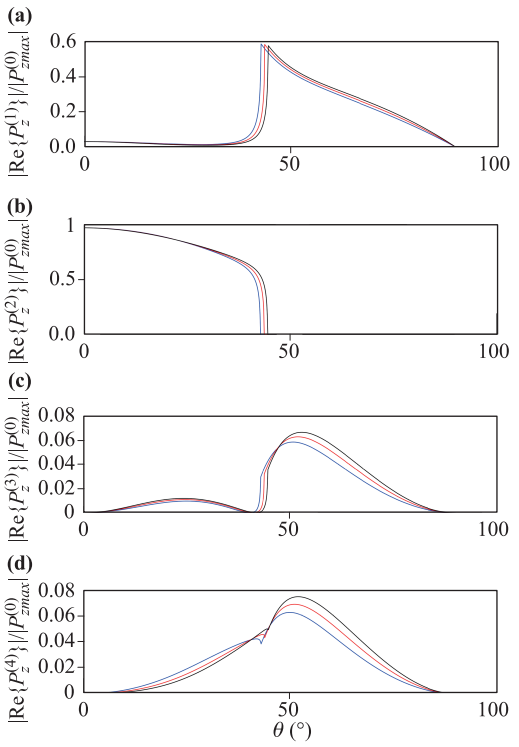


Fig. 12 $|\mathrm{Re}\{P_z^{(m)}\}|$ vs. θ for different values of $\delta^{*(1)}$ at $\varphi = 30°$, where blue, red and black curves stand for the cases of $\delta^{*(1)} = 0$, -0.073 and -0.127, respectively: **(a)** $|P_z^{(1)}|$ vs. θ; **(b)** $|P_z^{(2)}|$ vs. θ; **(c)** $|P_z^{(3)}|$ vs. θ; and **(d)** $|P_z^{(4)}|$ vs. θ.

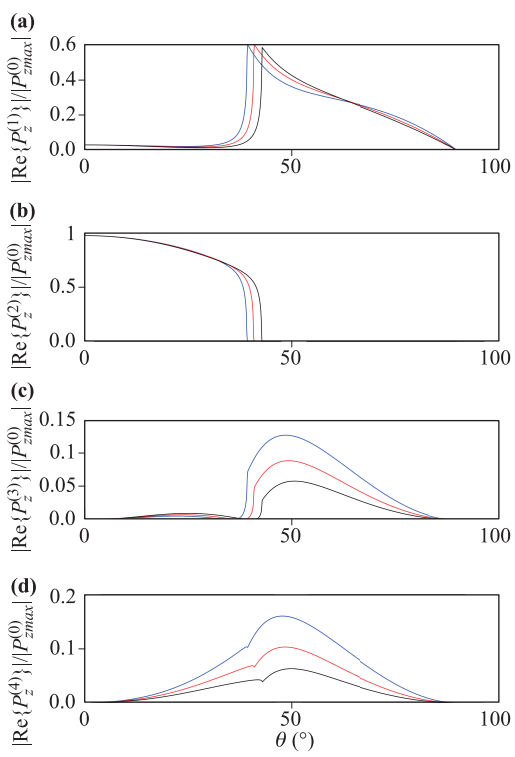


Fig. 11 $|\mathrm{Re}\{P_z^{(m)}\}|$ vs. θ for different values of $\varepsilon^{(1)}$ at $\varphi = 30°$, where blue, red and black curves stand for the cases of $\varepsilon^{(1)} = 0$, 0.103 and 0.2132, respectively: **(a)** $|P_z^{(1)}|$ vs. θ; **(b)** $|P_z^{(2)}|$ vs. θ; **(c)** $|P_z^{(3)}|$ vs. θ; and **(d)** $|P_z^{(4)}|$ vs. θ.

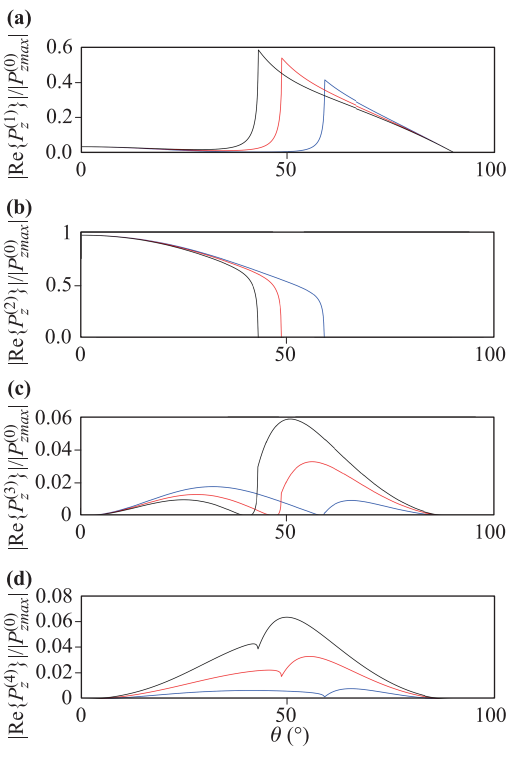


Fig. 13 $|\mathrm{Re}\{P_z^{(m)}\}|$ vs. θ for different values of $\varepsilon^{(2)}$ at $\varphi = 30°$, where blue, red and black curves stand for the cases of $\varepsilon^{(2)} = 0$, 0.103 and 0.2132, respectively: **(a)** $|P_z^{(1)}|$ vs. θ; **(b)** $|P_z^{(2)}|$ vs. θ; **(c)** $|P_z^{(3)}|$ vs. θ; and **(d)** $|P_z^{(4)}|$ vs. θ.

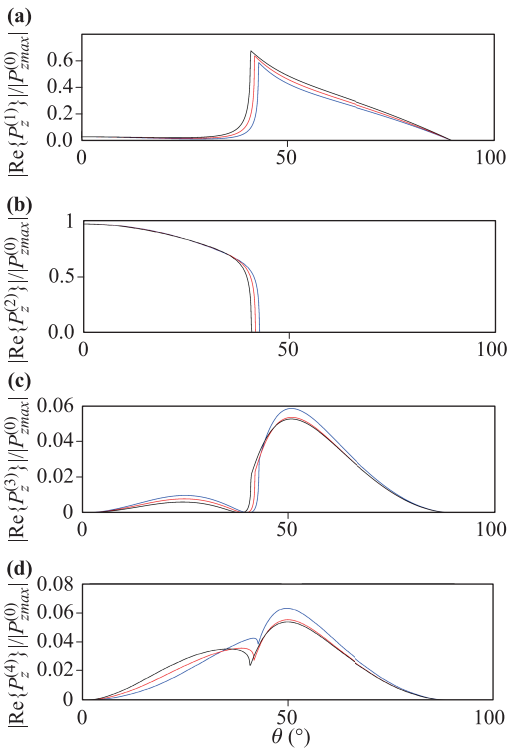


Fig. 14 $|\mathrm{Re}\{P_z^{(m)}\}|$ vs. θ for different values of $\delta^{*(2)}$ at $\varphi = 30°$, where blue, red and black curves stand for the cases of $\delta^{*(2)} = 0$, -0.073 and -0.127, respectively: **(a)** $|P_z^{(1)}|$ vs. θ; **(b)** $|P_z^{(2)}|$ vs. θ; **(c)** $|P_z^{(3)}|$ vs. θ; and **(d)** $|P_z^{(4)}|$ vs. θ.

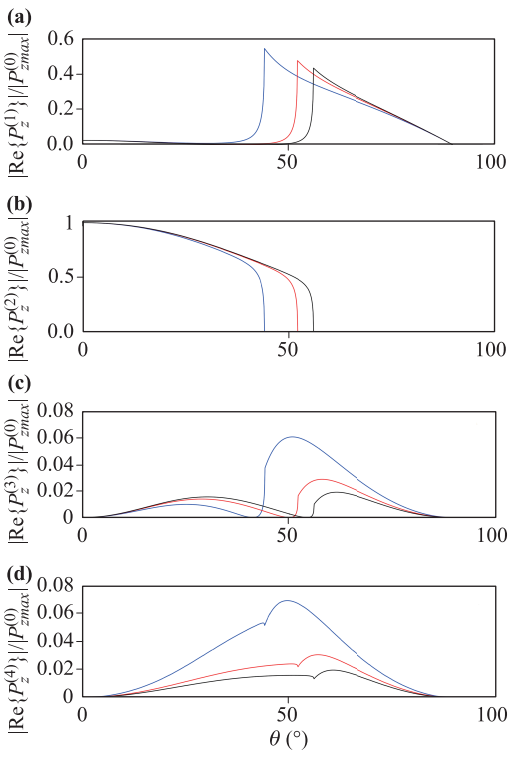


Fig. 15 $|\mathrm{Re}\{P_z^{(m)}\}|$ vs. θ for different values of φ, calculated from the parameters in Table 1, where blue, red and black curves stand for the cases of $\varphi = 0°$, $45°$ and $60°$, respectively: **(a)** $|P_z^{(1)}|$ vs. θ; **(b)** $|P_z^{(2)}|$ vs. θ; **(c)** $|P_z^{(3)}|$ vs. θ; and **(d)** $|P_z^{(4)}|$ vs. θ.

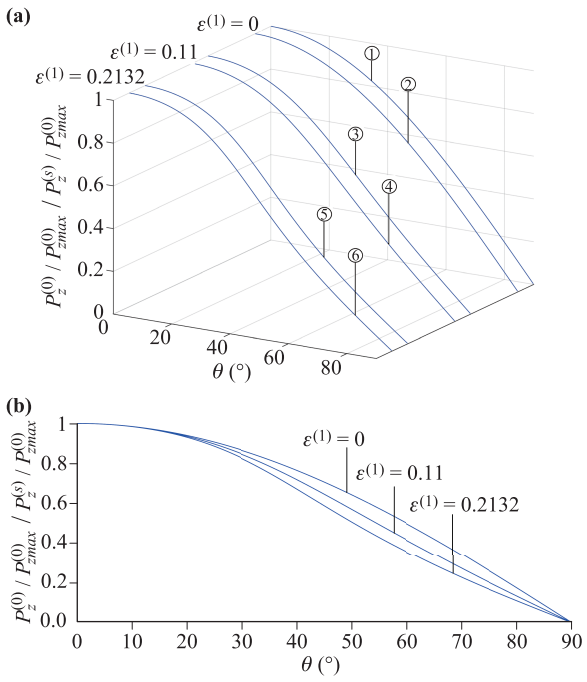


Fig. 16 $|\mathrm{Re}\{P_z^{(s)}\}|$ and $|P_z^{(0)}|$ vs. θ for several different values of $\varepsilon^{(1)}$ at $\varphi = 30°$: **(a)** three-dimensionure chart; **(b)** two-dimension chart.

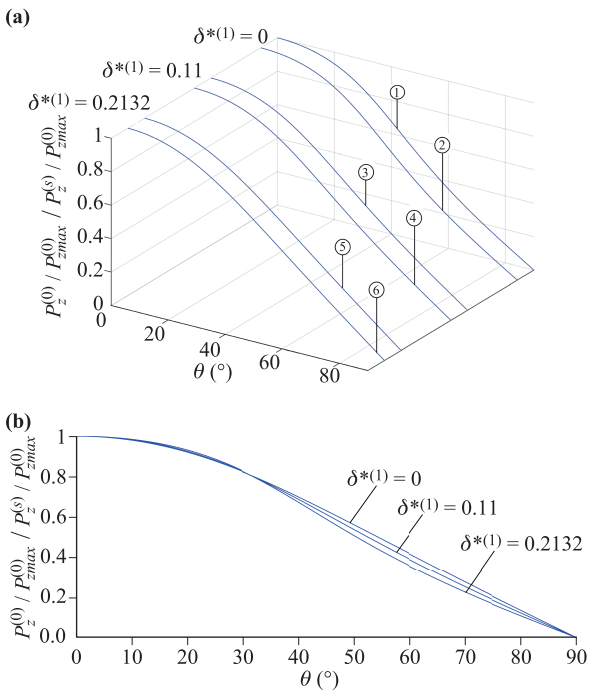


Fig. 17 $|\mathrm{Re}\{P_z^{(s)}\}|$ and $|P_z^{(0)}|$ vs. θ for several different values of $\delta^{*(1)}$ at $\varphi = 30°$: **(a)** three-dimension chart; **(b)** two-dimension chart.

The above-calculated results indicate that the values of either $|P_z^{(0)}|$ is influenced by the anisotropic parameters of the incidence (VTI) medium, but not by those of refraction (TTI) medium and tilt-angle.

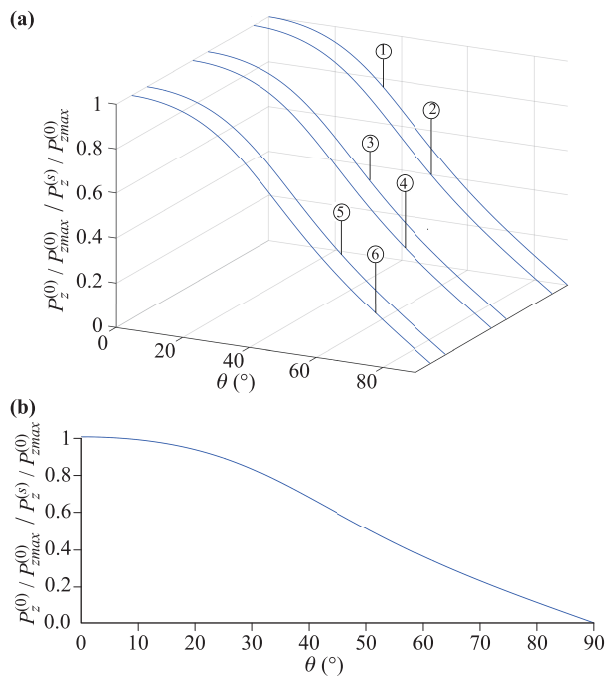


Fig. 18 $|\mathrm{Re}\{P_z^{(s)}\}|$ and $|P_z^{(0)}|$ vs. θ for several different values of $\varepsilon^{(2)}$, $\delta^{*(2)}$, and φ°, respectively: **(a)** three-dimension chart; **(b)** two-dimension chart. Where, curves ① and ② are three cases of $\varepsilon^{(2)} = 0$, $\delta^{*(2)} = 0$ and $\varphi = 0^\circ$, respectively; curves ③ and ④ are those of $\varepsilon^{(2)} = 0.11$, $\delta^{*(2)} = 0.11$ and $\varphi = 45^\circ$, respectively; and curves ⑤ and ⑥ are those of $\varepsilon^{(2)} = 0.2132$, $\delta^{*(2)} = 0.2132$ and $\varphi = 60^\circ$, respectively.

It is noted that in the pre-critical incident angle region, all induced waves are homogeneous and the z-components of their energy density fluxes are real (not complex). In the post-critical incident angle region, the reflection and refraction coefficients are purely complex; the reflected P- and SV-waves and the refracted SV-wave are homogenous and the z-components of their energy density fluxes become complex numbers. Meanwhile, the refracted P-wave becomes inhomogenous and the z-component of its energy density flux is purely imaginary. So, in the post-incident critical-angle region, $|\mathrm{Re}\{P_z^{(1,3,4)}\}| \neq |P_z^{(1,3,4)}|$ and $|\mathrm{Re}\{P_z^{(s)}\}| = |P_z^{(0)}| \neq |P_z^{(s)}|$.

Figures 16–18 show that curves ①, ③, and ⑤ are the same as the curves ②, ④, and ⑥, respectively, throughout all incident-angles. This indicates that the calculated reflection and refraction coefficients satisfy the law of energy conservation. Overall, regardless the variation of $\varepsilon^{(1)}$, $\delta^{*(1)}$, $\varepsilon^{(2)}$, $\delta^{*(2)}$, and φ, the summation $|\mathrm{Re}\{P_z^{(s)}\}|$ is always equal to $P_z^{(0)}$ for all incident angles, see Figs. 16–18.

4 Final remarks

We conclude this paper with the following remarks.

First of all, we have derived an eighth-order polynomial of refraction angle for refracted P- and SV-waves induced at VTI-TTI interface. This is achieved through Bond transformation. The analytical derivations of an eighth-order polynomial are confirmed from Snell's law through numerical calculations. An efficient algorithm is proposed in solving an eighth-order polynomial for calculations of reflection and refraction coefficients at VTI-TTI media interface.

The algorithm proposed in this report can be applied to calculations of reflection and refraction coefficients at VTI-TTI interface for all incident angle regions. The correctness of calculated reflection and refraction coefficients are verified by the law of energy conservation law.

Therefore, it is suitable for obtaining amplitude information of $R^{(1)}$ throughout incident-angles for AVO analysis of seismic exploration. It is also a good tool for phase information of $R^{(1)}$ in the post-critical-angle area to achieve the accurate time-depth conversion of seismic exploration data, as well as accurate measurement of P-wave propagation speed through the borehole wall in acoustic-logging.

From a VTI-TTI interface model with practical rock parameters, we have learned many aspects of VTI-TTI interface with the numerical calculations.

We found that for all incident angles the polarization coefficients of incident P-waves are always real, i.e., $u_x^{(0)}$ and $u_z^{(0)}$ are not complex. For incidence from pre-critical incidence angle region, the polarization coefficients of all induced waves are real, i.e., $u_x^{(m)}$ and $u_z^{(m)}$ are not complex, $m = 1$, 2, 3 and 4. For incidence from post-critical angle region, the polarization coefficients of reflected P- and SV-waves and refracted SV-wave are complex numbers, i.e., $u_x^{(m)}$ and $u_z^{(m)}$ are complex numbers, $m = 1$, 3 and 4; whereas the polarization coefficients of refracted P-wave are mixed ($u_x^{(2)}$ and $u_z^{(2)}$), one is real and the other is imaginary. The selection of real or imaginary of either $u_x^{(2)}$ or $u_z^{(2)}$ is determined by ellipse polarization rotational direction of the inhomogenous refracted P-wave.

The anisotropy of the incidence/refraction media and the tilt-angle of the refraction medium (TTI) would influence the amplitude and phase of reflection and refraction coefficients, as well as the location of the critical incidence angle $\theta_c^{(2)}$. Meanwhile, the reflection and refraction coefficients are not smooth continuous at $\theta = \theta_c^{(2)}$. The anisotropy of the incidence medium would influence the magnitude of power density flux of incident P-wave. The anisotropy and tile angle of the refraction medium influences the power density flux of each induced wave but does not influence the sum of power density fluxes of induced waves in z-direction. Finally, we note that the tilt-angle plays a more significant role in influencing reflection and refraction coefficients than that of anisotropy of the media.

Acknowledgements This work was supported in part by the National Natural Science Foundation of China (Grant No. 41974130) and by the Physical Sciences Division at The University of Chicago.

References

1. J. P. Castagna and M. M. Backus, Offset-Dependent Reflectivity — Theory and Practice of AVO Analysis, Society of Exploration Geophysicists Press, Tulsa, OK, USA, 1993
2. M. A. Mustapa, O. B. Yaakob, Y. M. Ahmed, C. K. Rheem, K. K. Koh, and F. A. Adnan, Wave energy device and breakwater integration: A review, *Renew. Sustain. Energy Rev.* 77, 43 (2017)
3. R. J. Przybyla, H. Y. Tang, A. Guedes, S. E. Shelton, B. E. Boser, and D. A. Horsley, 3D ultrasonic rangefinder on a chip, *IEEE. J. Solid-St. Circ.* 50(1), 320 (2015)
4. A. S. Goh, J. C. Kohn, D. B. Rootman, J. L. Lin, and R. A. Goldberg, Hyaluronic acid gel distribution pattern in periocular area with high-resolution ultrasound imaging, *Surg J.* 34(4), 510 (2014)
5. M. A. Breazeale, L. Adler, and G. W. Scott, Interaction of ultrasonic waves incident at the Rayleigh angle onto a liquid-solid interface, *J. Appl. Phys.* 48(2), 530 (1977)
6. A. Atalar, C. F. Quate, and H. K. Wickramasinghe, Phase imaging in reflection with an acoustic microscope, *Appl. Phys. Lett.* 31(12), 791 (1977)
7. R. Briers, O. Leroy, and G. Shkerdin, Bounded beam interaction with thin inclusions: Characterization by phase differences at Rayleigh angle incidence, *J. Acoust. Soc. Am.* 108(4), 1622 (2000)
8. G. L. Zhang, C. T. Hao, and C. Yao, A study of synthetic seismograms for SKS-wave response to crustal fractured-induce anisotropy, *Chin. J. Geophys.-Ch.* 59(7), 2498 (2016)
9. W. K. Cao, L. T. Wu, C. Zhang, J. C. Ke, Q. Cheng, T. J. Cui, and Y. Jing, Asymmetric transmission of acoustic waves in a waveguide via gradient index metamaterials, *Sci. Bull. (Beijing)* 64(12), 808 (2019)
10. Y. Wang, S. Y. Zhang, J. Xu, Y. C. Xie, and X. D. Lan, Characteristics of surface acoustic waves in (11$\bar{2}$0) ZnO film/R-sapphire substrate structures, *Sci. China Phys. Mech. Astron.* 61(2), 024311 (2018)
11. H. Zhang, S. Y. Yu, F. K. Liu, Z. Wang, M. H. Lu, X. B. Hu, Y. F. Chen, and X. G. Xu, Using coupling slabs to tailor surface-acoustic-wave band structures in photonic crystals consisting of pillars attached to elastic substrates, *Sci. China Phys. Mech. Astron.* 60(4), 044311 (2017)
12. Y. Y. Fu, Y. D. Xu, and H. Y. Chen, Negative refraction based on purely imaginary metamaterials, *Front. Phys.* 13(4), 134206 (2018)
13. S. G. Woon, Acoustical Imaging Techniques and Applications: Chapter 14, Negative Refraction, Acoustical Metamaterials and Acoustical Cloaking, John Wiley Sons, Ltd, 2012
14. L. Xu, Q. N. Wu, Y. Y. Zhou, and H. Y. Chen, Transformation devices with optical nihility media and reduced realizations, *Front. Phys.* 14(4), 42501 (2019)
15. K. Zoeppritz, Erdbebenwellen VIIIB, on the reflection and propagation of seismic waves, *Gottinger. Nachr.* 17(1), 66 (1919)
16. P. G. Richards and C. W. Frasier, Scattering of elastic waves from depth-dependent inhomogeneities, *Geophysics* 41(3), 441 (1976)
17. K. Aki and P. G. Richards, Quantitative Seismology: Theory and Methods, W. H. Freeman Press, New York, USA, 1980
18. R. T. Shuey, A simplification of the Zoeppritz equations, *Geophysics* 50(4), 609 (1985)
19. W. J. Ostrander, Plane-wave reflection coefficients for gas sands at nonnormal angles of incidence, *Geophysics* 49(10), 1637 (1984)
20. J. Y. Li, X. H. Chen, Z. J. Hao, and Z, H, Rui, A study on multiple time-lapse seismic AVO inversion, *Chin. J. Geophys-Ch.* 48(4), 902 (2005)
21. G. Z. Zhu, L. Liu, and D. Y. Fu, Experimental study on the non-specularly reflected ultrasonic beam on a liquid-solid interface, *Sci. China Ser. A* 44(2), 225 (2001)
22. L. Fa, L. Xue, Y. X. Fa, Y. L. Han, Y. D. Zhang, and H. S. Cheng, Acoustic Goos-Hanchen effect, *Sci. China Phys. Mech.* 60(10), 104311 (2017)
23. L. Thomsen, Weak elastic anisotropy, *Geophysics* 51(10), 1954 (1986)
24. Z. Wang, Seismic anisotropy in sedimentary rocks, part 1: A single-plug laboratory method, *Geophysics* 67(5), 1415 (2002)
25. Z. Wang, Seismic anisotropy in sedimentary rocks, part 2: Laboratory data, *Geophysics* 67(5), 1423 (2002)
26. G. L. Backus, Long-wave elastic anisotropy produced by horizontal layering, *J. Geophys. Res.* 67(11), 4427 (1962)
27. P. F. Daley and F. Hron, Reflection and transmission coefficients for transversely isotropic media, *Bull. Seismol. Soc. Am.* 67(3), 661 (1977)
28. P. F. Daley and F. Hron, Reflection and transmission coefficients for seismic waves in ellipsoidally anisotropic media, *Geophysics* 44(1), 27 (1979)
29. A. Rüger, P-wave reflection coefficient for transversely isotropic models with vertical and horizontal axes of symmetry, *Geophysics.* 1997, 62(14), 713 (1997)
30. I. Tsvankin, Seismic signature and analysis of reflection data in aisotropic media, Society of Exploration Geophysicists Press, Elsevier, Amsterdam, 2005
31. J. M. Carcione, Wave Fields in Real Media: Wave Propagation in Anisotropic, Anelastic and Porous Media, Elsevier Science Press, Amsterdam, 2001
32. L. Klimeš, Weak-contrast reflection-transmission coefficients in a generally anisotropic background, *Geophysics* 68(6), 2063 (2003)
33. L. Fa, R. L. Brown, and J. P. Castagna, Anomalous postcritical refraction behavior for certain transversely isotropic media, *J. Acoust. Soc. Am.* 120(6), 3479 (2006)
34. L. Fa, J. P. Castagna, and H. F. Dong, An accurately fast algorithm of calculating reflection/transmission coefficients, *Sci. China. Phys. Mech.* 51(7), 823 (2008)

35. B. A. Auld, Acoustic Fields and Waves in Solids, John Wiley & Sons Press, New York, USA, 1972
36. L. Fa, F. Y. Fa, Y. D. Zhang, P. F. Ding, J. M. Gong, G. H. Li, L. J. Li, S. J. Tang, and M. S. Zhao, Anomalous incident-angle and elliptical-polarization rotation of an elastically refracted P-wave, *Sci. Rep.* 5(1), 12700 (2015)
37. L. Fa, W. Y. Li, J. Zhao, Y. L. Han, M. Liang, P. F. Ding, and M. S. Zhao, Polarization state of an inhomogeneously refracted compressional-wave induced at interface between two anisotropic rocks, *J. Acoust. Soc. Am.* 141(1), 1 (2017)
38. L. Fa, M. S. Zhao, Y. C. Liu, L. Wang, Y. Q. Wang, and J. G. Sun, Polarization of plane wave propagating inside elastic hexagonal system solids, *Sci. China Phys. Mech. Astron.* 57(2), 251 (2014)
39. L. Fa, J. Zhao, Y. L. Han, G. H. Li, P. F. Ding, and M. S. Zhao, The influence of rock anisotropy on elliptical-polarization state of inhomogeneously refracted P-wave, *Sci. China Phys. Mech. Astron.* 59(4), 644301 (2016)
40. L. Fa, Z. Zeng, C. Deng, and M. S. Zhao, Effects of geometrical-size of cylindrical-shell transducer on acoustic-beam steering efficiency for a slim-hole acoustic-logging tool, *Open Acoustics Journal* 3(1), 21 (2010)
41. L. Fa, J. P. Castagna, Z. Zeng, R. L. Brown, and M. S. Zhao, Effects of anisotropy on time-depth relation in transversely isotropic medium with a vertical axis of symmetry, *Chin. Sci. Bull.* 55(21), 2243 (2010)
42. Y. Zhao, N. Zhao, L. Fa, and M. S. Zhao, Seismic signal and data analysis of rock media with vertical anisotropy, *J. Mod. Phys.* 04(01), 11 (2013)
43. L. Fa, L. Wang, Y. Zhao, L. Liu, Y. Zheng, N. Zhao, M. Zhao, and G. Li, Research progress in acoustical application to petroleum logging and seismic exploration, *Open Acoustics Journal* 6(1), 1 (2014)
44. L. Fa and M. S. Zhao, Recent development of an acoustic measurement system, in: Understanding Plane Waves, Nova Science Publishers, 2019
45. L. Fa and M. S. Zhao, Recent progress in acoustical theory and applications, in: Understanding Plane Waves, Nova Science Publishers, 2019